

1 **Structural controls on the location, geometry, and**  
2 **longevity of an intraplate volcanic system – The**  
3 **Tuatara Volcanic Field, Great South Basin, New**  
4 **Zealand**

5 <sup>1</sup>\*Thomas B. Phillips & <sup>2</sup>Craig Magee

6 <sup>1</sup>*Department of Earth Sciences, Durham University, Science Labs, Elvet Hill, Durham, DH13LE*

7 <sup>2</sup>*Institute of Geophysics and Tectonics, School of Earth Science and Environment, University of*  
8 *Leeds, Leeds, LS2 9JT, UK*

9 *\*Corresponding Author – thomas.b.phillips@durham.ac.uk*

10 **Abstract**

11 Intraplate volcanism is widely distributed across continents. Yet controls on the 3D geometry and  
12 longevity of individual volcanic systems remain poorly understood. Geophysical data provide insights  
13 into magma plumbing systems, but due to relatively low resolution, it is difficult to evaluate how  
14 magma transits highly heterogeneous continental interiors. We use borehole-constrained 2D seismic  
15 reflection data to characterise the 3D geometry of a volcanic field offshore New Zealand's South  
16 Island, termed the Tuatara Volcanic Field, and investigate its relationship with pre-existing structure.  
17 The ~270km<sup>2</sup> field is dominated by a dome-shaped lava edifice, surrounded and overlain by ~69  
18 volcanoes and >70 sills emplaced over 40 Myr from the Late Cretaceous to Early Eocene (~85 Ma–45  
19 Ma). The Tuatara Volcanic Field is located above a basement terrane boundary represented by the  
20 Livingstone Fault; the recently active Auckland Volcanic Field is similarly located along-strike on the  
21 North Island. We suggest the Livingstone Fault controlled the location of the Tuatara Volcanic Field  
22 by producing relief at the base lithosphere, thereby focussing lithosphere detachment over ~40 Myr,

23 and provided a pathway that facilitated magma ascent. We highlight how observations from ancient  
24 intraplate volcanic systems may inform our understanding of active intraplate volcanic systems,  
25 including the Auckland Volcanic Field.

## 26 **1 Introduction**

27 Intraplate volcanism encompasses igneous activity away from and unrelated to plate boundary  
28 processes (e.g. subduction and mid-ocean ridge spreading). Such intraplate volcanic systems develop  
29 in a variety of forms, from the construction of volcanic chains (e.g., Davies et al., 2015), through to  
30 large caldera forming eruptions (e.g., Timm et al., 2009) or the formation of volcanic fields  
31 comprising small, relatively short-lived volcanoes (e.g., Németh, 2010; Németh et al., 2003; Reynolds  
32 et al., 2018). These different styles of volcanic activity reflect the range of processes that drive, and  
33 influence the location and longevity of, intraplate volcanism. For example, hotspot intraplate  
34 volcanism occurs above a fixed, thermal mantle anomaly, producing chains of extinct volcanoes as  
35 plate motion carries active volcanoes away from the melt source (e.g., Clague and Jarrard, 1973;  
36 Morgan, 1972; Sleep, 1992). In contrast, during continental rifting, the location and longevity of  
37 intraplate volcanic systems relates to the location and magnitude of lithospheric thinning (e.g., Wilson  
38 et al., 1995; Wu et al., 2018). In other intraplate settings, such as the Turkish-Iranian Plateau, Eastern  
39 Australia, or Zealandia, diffuse volcanism occurs seemingly randomly over wide (continental-scale)  
40 areas (e.g., Finn et al., 2005; Hoernle et al., 2006; Kaislaniemi et al., 2014; Rawlinson et al., 2017).  
41 Whilst records of intraplate volcanism across these broad areas may be relatively continuous,  
42 individual volcanic systems are typically active across much shorter (Myr) timescales. Relative to  
43 hotspot- or rift-related intraplate volcanism, the processes driving the formation of these diffuse  
44 volcanic fields are often elusive and we particularly poorly understand the factors controlling the  
45 distribution and longevity of individual volcanic systems (e.g. Valentine and Hirano, 2010). In the  
46 absence of a clear process-driven control on the distribution of intraplate volcanic fields, pre-existing  
47 lithospheric and/or crustal structures may represent a crucial and commonly overlooked influence on  
48 their siting, magma plumbing system structure, and longevity.



49 Constraining the 3D geometry of magma plumbing systems and assessing how intraplate volcanism  
50 relates to and/or may be influenced by pre-existing structures is difficult because (see Magee et al.,  
51 2018 and references therein): (i) geophysical and geodetic data typically provide only a relatively low  
52 resolution view of subsurface magma or igneous rock distribution, and capture little information on  
53 host rock structure; (ii) outcrop analyses of ancient plumbing systems allow detailed analyses of  
54 intrusion geometry and host rock structure, but limitations in exposure at Earth's surface mean we  
55 cannot often place these observations within a 3D context; and (iii) petrological and chemical data,  
56 whilst providing crucial insights into melt and magma evolution, are often interpreted within a poorly  
57 defined structural framework. Reflection seismology provides a powerful tool for imaging the 3D  
58 geometry of volcanoes and magma plumbing systems in the subsurface (e.g., Bischoff et al., 2017;  
59 Bischoff et al., preprint; Buntin et al., 2019; Magee et al., 2019; Magee et al., 2016; McLean et al.,  
60 2017; Morley, 2018; Quirie et al., 2019; Reynolds et al., 2017; Sun et al., 2019a).

61 Here, we use borehole-constrained seismic reflection data to investigate the 3D structure of an  
62 intraplate volcanic field buried within the Great South Basin, offshore of the South Island of New  
63 Zealand. The volcanic field comprises a ~270 km<sup>2</sup> central edifice, formed of stacked lavas,  
64 surrounded and overlain by at least 69 volcanic cones developed at varying stratigraphic levels; we  
65 also identify a network of >70 igneous sills that formed the shallow-level plumbing system and linked  
66 to individual volcanoes. We refer to this province as the 'Tuatara Volcanic Field' after the endemic  
67 New Zealand reptile, the name of which is derived from the Māori language and fittingly means  
68 'peaks on the back'. The well exposed and studied basement geology onshore New Zealand (e.g.,  
69 Mortimer, 2004; Tarling et al., 2019), combined with a detailed and comprehensive record of  
70 intraplate volcanism throughout the Cenozoic (e.g., Adams, 1983; Bischoff et al., preprint; Cooper et  
71 al., 1987; Hoernle et al., 2006; Németh and White, 2003; Rout et al., 1993; Speight, 1943; Stipp and  
72 McDougall, 1968; Waight et al., 1998) and high-resolution marine geological and geophysical data  
73 available in the offshore domain (e.g., Mortimer et al., 2002; Phillips and McCaffrey, 2019; Tulloch et  
74 al., 2019; Uruski, 2015; Uruski et al., 2007), allow us to fully characterise and constrain the internal  
75 architecture of the Tuatara Volcanic Field and assess how it relates to the surrounding crustal

76 structure. By identifying seismic-stratigraphic onlap and downlap relationships, we show the  
77 volcanoes and sills were emplaced between ~85 and ~45 Ma, recording ~40 Myr of punctuated  
78 igneous activity spanning the Late Cretaceous-to-Early Eocene.

79 We propose the location and longevity of the Tuatara Volcanic Field was controlled by the underlying  
80 terrane boundary marked by the Livingstone Fault. In particular, we suggest changing relief of the  
81 lithosphere-asthenosphere boundary across the terrane boundary promoted local lithospheric  
82 detachment and melting, whilst the Livingstone Fault facilitated magma ascent. The structural setting  
83 of the Tuatara Volcanic Field is equivalent to that of the recently active Auckland Volcanic Field on  
84 the North Island (active 193 Ka - 500 y BP; Hopkins et al., 2020; Lindsay et al., 2011). Our study of  
85 the Tuatara Volcanic Field, which highlights how pre-existing structure and sill-complex development  
86 can influence the location and longevity of volcanic activity, may offer important insights into the  
87 processes occurring at the Auckland Volcanic Field and intraplate volcanism elsewhere.

88

## 89 **2 Geological setting**

90 Zealandia is an ideal natural laboratory to explore how crustal structure may affect the distribution,  
91 geometry, and evolution of volcanic fields: it hosts a long record of intraplate volcanism, from the  
92 Cenozoic to present day, dispersed across the length and breadth of a continent comprising a  
93 heterogeneous basement formed of multiple distinct terranes (e.g., Mortimer, 2004; Mortimer et al.,  
94 2002; Mortimer et al., 1999; Phillips and McCaffrey, 2019; Tulloch et al., 2019). This study focusses  
95 on a ~10,000 km<sup>2</sup> area in the northern part of the Great South Basin, offshore the east coast of the  
96 South Island of New Zealand and located 60 km SE of the Dunedin Volcano on the Otago Peninsula  
97 (Figure 1). The study area forms part of the Campbell Plateau on the continental shelf of Zealandia, an  
98 extensive area of submerged and extended continental crust characterised by water depths of ~500–  
99 1500 m (Adams, 1962).

### 100 **2.1 Regional geological evolution**

101 The basement geology of New Zealand comprises the Austral Superprovince, which incorporates a  
102 series of terranes that accreted along the southern margin of Gondwana between the Cambrian-to-  
103 Cretaceous (e.g., Bishop et al., 1985; Howell, 1980; Johnston, 2019; Mortimer, 2004; Mortimer et al.,  
104 2014). These terranes are divided into the Eastern and Western provinces, which are separated by the  
105 Median Batholith (Figure 1) (Mortimer, 2004; Mortimer et al., 1999). Projecting onshore terrane  
106 boundaries offshore along-strike suggests the study area resides within the Eastern Province and spans  
107 the faulted boundary between the Caples Terrane and the Dun Mountain-Maitai Terrane (Figure 1).  
108 This terrane boundary corresponds to the Livingstone Fault (Figure 1), which is a serpentinite-  
109 dominated shear zone that ranges from 10's to 100's of metres wide, dips steeply to the northeast, and  
110 extends down to, at least, the base of the crust (Mortimer et al., 2002; Tarling et al., 2019). The Caples  
111 Terrane comprises weakly metamorphosed volcanoclastic greywackes, which accreted to the southern  
112 margin of Gondwana during the Permian-to-Triassic (Johnston, 2019; Mortimer, 2004; Robertson et  
113 al., 2019), whilst the Dun Mountain-Maitai Terrane includes the Early Permian Dun Mountain, mafic-  
114 to-ultramafic ophiolite belt and an overlying, 6 km thick sequence of Late Permian-Middle Triassic  
115 volcanoclastic sedimentary rocks (i.e. the Maitai Group; Mortimer, 2004). Due to its mafic/ultramafic  
116 lithology, the Dun Mountain ophiolite is delineated by the Junction Magnetic Anomaly, which forms  
117 a ~20 km wide positive anomaly onshore (e.g., Davey and Christoffel, 1978; Sutherland, 1999;  
118 Tulloch et al., 2019), but is less prominent offshore (Figure 2). Further positive magnetic anomalies,  
119 forming part of the Stokes Magnetic Anomaly System, are identified south of the Junction Magnetic  
120 Anomaly and likely relate to the Rotoroa igneous province and additional volcanics within the Eastern  
121 Province terranes (Figure 2) (Grobys et al., 2009; Hunt, 1978; Sutherland, 1999; Woodward and  
122 Hatherton, 1975).

123 Subduction and terrane accretion along the southern margin of Gondwana ceased during the mid-to-  
124 late Cretaceous as the Hikurangi Plateau, part of a Large Igneous Province, collided with and jammed  
125 the subduction zone (Davy et al., 2008). Following the cessation of subduction, Zealandia underwent  
126 two major phases of rifting related to the breakup of Gondwana during the Late Cretaceous (Figure  
127 1B) (Kula et al., 2007; Laird and Bradshaw, 2004; Mortimer et al., 2019; Tulloch et al., 2019; Uruski

128 et al., 2007). Initial rifting from ~100–90 Ma related to break-up between Zealandia and Australia,  
129 and may have led to extensional reactivation of terrane boundaries beneath the proto-Great South  
130 Basin (Figure 1) (Phillips and McCaffrey, 2019). The second rift phase occurred from ~90–80 Ma in  
131 response to extension between Zealandia and Western Antarctica, resulting in the formation of the  
132 NE-trending Great South and Canterbury basins (Figure 1) (Beggs, 1993; Grobys et al., 2009; Kula et  
133 al., 2007; Tulloch et al., 2019).

134 The Alpine Fault formed during the Early Cenozoic to accommodate plate motion between the Pacific  
135 and Australian plates. Although located relatively close (~200 km) to the Alpine Fault between the  
136 Pacific and Australian plates, the Great South and Canterbury basins were relatively tectonically  
137 stable, and not influenced by back-arc extension or Alpine deformation, following Late Cretaceous  
138 rifting. The Alpine Fault offset the basement terranes across Zealandia, such that those beneath the  
139 South Island are also present beneath parts of the North Island (e.g. Cassidy and Locke, 2010;  
140 Collanega et al., 2018; Cooper and Norris, 1994; Howell, 1980; Lamb et al., 2016; Muir et al., 2000;  
141 Tarling et al., 2019). In particular, the Dun Mountain-Maitai and Caples terranes, which underlie our  
142 study area, are present beneath the Auckland Volcanic Field in the North Island (Figure 1) (Cassidy  
143 and Locke, 2010; Hopkins et al., 2020; Le Corvec et al., 2013; McGee et al., 2013; Spörli et al.,  
144 2015).

145 Late Cretaceous syn-rift strata within the Great South Basin, which were deposited unconformably  
146 onto the Permian-to-Triassic crystalline basement of the Caples and Dun Mountain-Maitai terranes,  
147 are dominated by siliciclastic rocks and coal measures of the Hoiho Group (Figure 1b) (Higgs et al.,  
148 2019; Killops et al., 1997; Sahoo et al., 2014). Widespread deposition of deep marine mudstones and  
149 siltstones occurred across the majority of the Great South and Canterbury Basins during the Cenozoic,  
150 with some carbonate deposition in the Oligocene-Miocene (Fig. 1b) (Bertoni et al., 2019; Chenrai and  
151 Huuse, 2020; Morley et al., 2017). The Marshall Paraconformity forms the Oligocene-Eocene  
152 boundary across the area and is purported to be related to the onset of the Antarctic circumpolar  
153 current (Fulthorpe et al., 1996; Morley et al., 2017). Much of the shallow stratigraphy across the Great  
154 South and Canterbury Basins has been reworked into contourite deposits (Figure 1b) (Fulthorpe et al.,

155 1996; Lu and Fulthorpe, 2004). At the present day, a series of steep-sided canyons traverse the seabed  
156 across the area, often eroding down to the Marshall Paraconformity surface (Figure 1b).

157

## 158 **2.2 Intraplate igneous activity across Zealandia**

159 Following the breakup of Gondwana in the Late Cretaceous, widespread and long-lived magmatic and  
160 volcanic activity has occurred in intraplate settings across Zealandia. Aside from back-arc rifting and  
161 associated volcanism in the Taupo Volcanic Zone (1.5 Ma–Present), examples of Late Cretaceous  
162 and/or Cenozoic intraplate volcanic systems include: the Auckland Volcanic Field (193 Ka – 500 y  
163 BP) on the North Island (Acocella et al., 2003; Cassidy and Locke, 2010; Hopkins et al., 2020; Le  
164 Corvec et al., 2013; McGee et al., 2013); and the Akaroa and Lyttleton volcanoes (12-6 Ma), and the  
165 Dunedin Volcano (16-11.7 Ma) of the Banks and Otago Peninsulas, respectively, on the South Island  
166 (Figure 1) (Price and Chappell, 1975; Speight, 1943; Stipp and McDougall, 1968). Offshore New  
167 Zealand, the Auckland (~37–19, 25–12 Ma) and Chatham islands (85–82, 41–35, 6–3 Ma) located  
168 towards the eastern and southern margins of Zealandia, respectively, were also repeatedly active  
169 during the Late Cretaceous-to-Cenozoic (Adams, 1983; Grindley et al., 1977), with further magmatic  
170 and volcanic activity having been documented in the Canterbury and Taranaki basins during the  
171 Miocene (Bischoff et al., preprint; Bischoff et al., 2017; Morley, 2018; Reeves et al., 2018). A  
172 detailed catalogue of the timings of intraplate volcanism across Zealandia can be found in Hoernle et  
173 al. (2006) and Timm et al. (2010), and references therein, with further examples of intraplate  
174 volcanism shown in Figure 1a.

175 The causal mechanism for the diffuse Cenozoic-to-present record of intraplate volcanic activity across  
176 Zealandia is difficult to reconcile with fixed hotspot- and rift-related processes (Timm et al., 2010).  
177 For example, volcanic activity is not compatible with a plume-related origin as such a long record of  
178 activity would require a static Zealandia relative to a ‘fixed’ mantle source; yet plate motion data  
179 indicate Zealandia has moved ~4000 km N/NW during the Cenozoic (Clouard and Bonneville, 2005;  
180 Hoernle et al., 2006; Sutherland, 1995; Wright et al., 2016). Furthermore, aside from igneous activity

181 related to back-arc rifting in the Taupo Volcanic Zone, Cenozoic magmatism across Zealandia is not  
182 related to lithospheric thinning and extension, which ceased during the Late Cretaceous (Figure 1b)  
183 (Acocella et al., 2003; Kula et al., 2007; Laird and Bradshaw, 2004; Mortimer et al., 2019). The  
184 igneous rocks sampled onshore New Zealand also show an OIB-type affinity not compatible with rift-  
185 related magmatism; their composition, including silica-undersaturated nephelinites and basanites,  
186 suggests they were derived from an asthenospheric source with varying degrees of input from a  
187 metasomatised mantle lithosphere (Finn et al., 2005; Hoernle et al., 2006). Intraplate volcanism across  
188 Zealandia is instead proposed to relate to localised detachment of dense material from the base of the  
189 lithosphere, small-scale convection, and decompression melting of upwelling asthenosphere (Elkins-  
190 Tanton, 2005; Hoernle et al., 2006; Timm et al., 2009; Timm et al., 2010). As a driver for lithosphere  
191 detachment, it has been suggested that the lithosphere beneath Zealandia contains large amounts of  
192 garnet pyroxenites and eclogites following protracted subduction, creating a contrast between dense  
193 lower lithosphere and relatively less dense upper asthenosphere (Elkins-Tanton, 2005; Hoernle et al.,  
194 2006; Timm et al., 2009). Similarly, increased mantle water content in a post-subduction setting may  
195 decrease mantle viscosity and lower the peridotite solidus, resulting in small-scale convection at the  
196 base of the lithosphere (Elkins-Tanton, 2005; Kaislaniemi et al., 2014). A key component of this  
197 coupled lithosphere detachment and small-scale convection mechanism is that the magma source is  
198 not fixed in specific locations in the mantle or lithosphere, allowing individual intraplate volcanic  
199 systems to occur over widespread areas and long timescales.

## 200 **3 Data and methods**

### 201 **3.1 Available data and seismic interpretation**

202 In this study, we use 2D seismic reflection data from three different surveys (OMV, DUN and HUN),  
203 with a total line length of >50,000 km. These datasets were acquired over a range of years (1972,  
204 2006, and 2008) and, accordingly, have different acquisition and processing parameters. Two of the  
205 surveys (OMV, DUN) record to ~8 s two-way travel-time (TWT), whilst the HUN survey records to  
206 ~5 s TWT. Seismic lines are typically oriented either NE-SW or NW-SE, and have a maximum

207 spacing of 2 km in the NE direction and ~8 km in the NW direction (Figure 2). All seismic data are  
208 zero phase and displayed in normal polarity, such that a downward increase in acoustic impedance  
209 (e.g., the seabed) is represented by a peak (red) reflection, with a downward decrease in acoustic  
210 impedance represented by a trough (blue). The seabed across the study area is cut by multiple, steep-  
211 sided, up to ~0.5 s TWT deep canyons, which often produce geophysical artefacts (multiples) at  
212 deeper stratigraphic levels that partially obscure reflection configurations. There are no boreholes in  
213 the study area but we tie our seismic data to the Toroa-1 well, located ~140 km to the SW, to  
214 constrain ages of key stratigraphic units (Figure 1a). The magnetic data used in this study are shown  
215 as reduced to pole in order to place the anomalies vertically above the magnetic source (Figure 2).

### 216 **3.2 Seismic resolution**

217 The limit of separability (wavelength ( $\lambda$ )/4) within the sedimentary succession of interest, based on an  
218 average seismic velocity of ~3 km s<sup>-1</sup> for the stratigraphic sequence derived from the Toroa-1  
219 borehole (Figure 1) and an average dominant frequency of ~30 Hz, is ~25 m; the limit of visibility  
220 ( $\lambda/30$ ), i.e. the thinnest structure that will be detected in the data, is ~3 m (Slatt, 2006). Features  
221 imaged in the seismic data that are thicker than the limit of separability will produce discrete  
222 reflections that can be linked to their top and base, whilst features with a thickness between the limits  
223 of separability and visibility will be displayed as tuned seismic reflection packages (Kallweit and  
224 Wood, 1982; Widess, 1973). Such tuned reflection packages occur because reflections from the top  
225 and base of the same feature interfere on their return to the surface and cannot be deconvolved  
226 (Brown, 2011).

227 No igneous features associated with the Tuatara Volcanic Field are penetrated by boreholes, so we do  
228 not know their composition or seismic velocity. However, based on comparison to the Maahunui  
229 Volcanic Field located in the northern Canterbury Basin, where the Resolution-1 boreholes intersect  
230 a gabbroic sill (Bischoff et al., 2020; Bischoff et al., 2019; Magee et al., 2019), and to volcanic fields  
231 sampled onshore New Zealand (Hoernle et al., 2006; Németh and White, 2003; Timm et al., 2009),  
232 we infer the Tuatara Volcanic Field is likely dominantly mafic. From an average interval velocity of  
233 ~5.2 km s<sup>-1</sup> for the gabbroic sill intersected by Resolution-1 (Magee et al., 2019), coupled with

234 estimated velocity ranges for mafic volcanic fields imaged in seismic reflection data elsewhere (e.g.,  
235 western India -  $\sim 3.3\text{--}5.5\text{ km s}^{-1}$ , Calvès et al. (2011); Australia, Bight Basin -  $\sim 2.4\text{--}6.7\text{ km s}^{-1}$ , Magee  
236 et al. (2013b); Australia, Bass Basin -  $2.2\text{--}4.0\text{ km s}^{-1}$ , Reynolds et al. (2018)), we anticipate that  
237 igneous rocks within the Tuatara Volcanic Field likely have an average seismic velocity of  $4.5\pm 1.5$   
238  $\text{km s}^{-1}$ . Combined with a dominant seismic frequency of  $\sim 30\text{ Hz}$  within the depth interval of the  
239 Tuatara Volcanic Field, our inferred velocities correspond to limits of separability and visibility of  
240  $\sim 25\text{--}50\text{ m}$  and  $3\text{--}7\text{ m}$ , respectively. As we do not know the detailed velocity structure of the volcanic  
241 province and surrounding strata, particularly its lateral variability, we do not depth-convert the  
242 seismic reflection data and present measurements in time rather than depth to avoid additional errors.

### 243 **3.3 Interpreting and dating volcano-magmatic features**

244 We identify and map a series of different igneous sills, lavas, and volcanoes across the study area  
245 based on their (e.g. Eide et al., 2018; Planke et al., 2005; Planke et al., 2000; Symonds et al., 1998;  
246 Thomson, 2005): (i) relatively high amplitude compared to stratigraphic reflections; (ii) positive  
247 polarity; (iii) limited lateral extent; and (iv) geometrical similarity to sills, lavas, and volcanoes  
248 observed elsewhere. Sills were also mapped based on whether their corresponding reflection cross-  
249 cuts, but does not offset background stratigraphic reflections (e.g. Magee et al., 2016; Planke et al.,  
250 2005; Thomson and Hutton, 2004). To constrain the relative age of inferred volcano-magmatic  
251 features, we mapped five stratigraphic horizons across the area that we correlated to the Tara-1 and  
252 Toroa-1 wells located  $\sim 130\text{--}140\text{ km}$  to the south (Figure 1 and Supplementary Figure 1): Top  
253 Coniacian ( $\sim 86.3\text{ Ma}$ ); Top Cretaceous ( $\sim 66\text{ Ma}$ ); Top Paleocene ( $\sim 56\text{ Ma}$ ); Top Early Eocene ( $\sim 45.7$   
254  $\text{Ma}$ ); and the Marshall Paraconformity (Base Oligocene  $\sim 33.9\text{ Ma}$ ). There is no well control on deeper  
255 stratigraphic levels throughout the Great South Basin, although a tentative top crystalline basement,  
256 corresponding to a high-amplitude reflection separating overlying continuous reflections from  
257 underlying chaotic reflectivity, is interpreted on individual sections (Sahoo et al., 2014; Uruski et al.,  
258 2007; Uruski, 2010). From these mapped stratigraphic horizons, we can constrain the relative timing  
259 of emplacement of different igneous features by: (i) determining the age interval of strata that  
260 interpreted volcanoes and lavas were erupted onto (i.e. the syn-volcanic palaeosurface), and the age



261 interval of strata that directly overlies and onlaps onto them (e.g. Magee et al., 2013b; Symonds et al.,  
262 1998); (ii) dating strata encasing sills, which the intrusions must post-date; and (iii) defining the age  
263 of strata onlapping onto intrusion-induced forced folds above sills, where observed, which formed at  
264 the contemporaneous free surface to accommodate sill intrusion (Hansen and Cartwright, 2006;  
265 Magee et al., 2017; Reeves et al., 2018; Trude et al., 2003).

266 As only 2D seismic reflection data are available, many volcano-magmatic features are only observed  
267 on individual 2D lines, meaning we cannot assess or quantify their individual 3D geometry. Where  
268 volcano-magmatic features can confidently be mapped across several 2D lines, we utilise the seismic  
269 software to interpolate our 2D horizon interpretations and recover their approximated 3D structure  
270 (see Hansen et al., 2008). Whilst this interpolation technique is broadly applied to extract information  
271 on the 3D geometry of volcanoes and sills imaged in 2D seismic reflection, the 2D seismic lines may  
272 not intersect the centre or maximum diameter of any specific feature (e.g., Hansen et al. 2008; Magee  
273 et al. 2013). Furthermore, we acknowledge that seemingly isolated features interpreted on different  
274 sections may in fact form part of a larger, singular structure. Quantitative measurements can therefore  
275 only be considered to represent minimum estimates. Finally, we note that some small volcano-  
276 magmatic features present in the study area may occur between and thus not be imaged by our 2D  
277 seismic grid.

278

## 279 **4 Identification of volcano-magmatic structures in the Tuatara**

### 280 **Volcanic Field**

281 We recognise a variety of different intrusive and extrusive igneous features that we can differentiate  
282 based on their location relative a central structural high, which we term the ‘Central edifice’. For  
283 clarity, here we sequentially describe and interpret the origin and age of: (i) high-amplitude  
284 reflectivity comprising the Central edifice; (ii) mound-like structures atop and beyond the lateral

285 limits of the Central edifice; and (iii) intrusive features, and associated host rock structures, beyond  
286 the lateral limits of the main edifice.

287

## 288 **4.1 Central edifice**

### 289 *4.1.1 Observations*

290

291 The Tuatara Volcanic Field is characterised by a ~0.5 s TWT thick package of stacked, broadly sub-  
292 parallel, high-amplitude seismic reflectivity that thins towards its margins and forms a convex-  
293 upwards domal structure (Figures 2, 3, 4); we term this the Central edifice. The top of the reflection  
294 package has a positive polarity, indicating it corresponds to a downwards increase in acoustic  
295 impedance (e.g., Figs 3, 4). Beneath this high-amplitude reflection package, seismic reflections appear  
296 dimmer and more chaotic (i.e. they are ‘washed out’) compared to areas at the same structural level  
297 beyond the lateral limits of the Central edifice (Figs 3, 4). Despite the poorer imaging beneath the  
298 high-amplitude reflection package, we are able to tentatively map the underlying top acoustic  
299 basement and, occasionally, the Top Coniacian and Top Cretaceous horizons (Figs 3, 4); we note that  
300 the most prominent reflections often correspond to seafloor canyon-related multiples (Fig. 3). Some  
301 offset reflections across potential faults can also be tentatively identified on individual seismic  
302 sections (Figure 3).

303 In plan-view, the high-amplitude reflection package defining the Central edifice displays an elliptical  
304 geometry, covering ~270 km<sup>2</sup>, with a NW-trending long axis 23 km in length and a 15 km long, NE-  
305 trending short axis (Figure 2b). The upper surface of the high-amplitude reflection package reaches 2  
306 s TWT at its shallowest point in the centre and deepens to 2.5–3 s TWT around its margins (Figures  
307 2b, 3, 4). At the deepest part of its upper surface, Upper Cretaceous strata onlap onto the high-  
308 amplitude reflection package (Figure 3), whilst at shallower depths it is onlapped and overlain by  
309 Early Eocene strata. In places, the top Paleocene horizon can be mapped through the upper portion of  
310 the high-amplitude reflection package (Figure 3, 4).

311 We also identify some areas of lower amplitude reflectivity within the reflection package, which  
312 typically correspond to mound-shaped features (see section 4.2), or reflections displaying a clinofor-  
313 like geometry (Figs 3, 4); i.e. they consist of gently dipping reflections with a sigmoidal geometry  
314 <100 ms TWT high. The top inflexion point of these sigmoidal reflections is typically horizontal  
315 across the reflection package (Figure 5).

#### 316 ***4.1.2 Interpretation***

317

318 We interpret the domal package of high-amplitude reflectivity as a series of stacked, tabular lava  
319 sequences based on: i) the high-amplitude and positive polarity of the reflections, consistent with a  
320 downwards increase in acoustic impedance from lower velocity ( $\sim 3 \text{ km s}^{-1}$ ), lower density  
321 sedimentary rocks above into higher velocity ( $\sim 4.5 \text{ km s}^{-1}$ ), higher density igneous lavas; ii) the  
322 inference that underlying reflections locally display a convex-upwards morphology, which could be a  
323 geophysical velocity ‘pull-up’ artefact akin to those observed beneath volcanoes elsewhere and  
324 related to seismic energy travelling through an overlying high velocity layer (e.g. Magee et al.,  
325 2013b; Sun et al., 2019a); iii) the lack of reflectivity beneath the package, as high impedance lavas  
326 can scatter and attenuate seismic energy, restricting imaging of underlying layers (e.g. Gallagher and  
327 Dromgoole, 2007; Maresh et al., 2006); and iv) the laterally discontinuous nature of the reflections,  
328 forming an isolated domal structure, suggestive of a non-sedimentary origin (Figure 3, 4). Similarities  
329 between the seismic expression of tabular lava sequences identified and confirmed by boreholes  
330 elsewhere and the domal high-amplitude reflection package we observed, supports our interpretation  
331 that the Central edifice comprises a stacked lava sequence (McLean et al., 2017; Quirie et al., 2019;  
332 Walker et al., 2019). Our tentative interpretation that normal faults can be recognised beneath the  
333 high-amplitude reflection package suggests that the edifice was erupted atop a horst-like structure  
334 formed during earlier rifting; this inference remains contentious as we are unable to correlate  
335 interpreted faults across multiple seismic sections and thus cannot confirm the basement structure  
336 (Figure 3, 4). We suggest this pre-existing horst-like structure likely formed a partly buried, structural  
337 high during volcanism, with extrusion preferentially occurring towards its top surface, where the lavas  
338 are thickest (Figure 3, 4).

339 Based on their location within and associated with the stacked lava sequences, we suggest the  
340 relatively low-amplitude, sigmoidal reflection packages may also be igneous in origin. In particular, we  
341 consider these sigmoidal reflection packages correspond to lava or hyaloclastite deltas, as they appear  
342 similar in their geometry, structural setting, and seismic character to examples identified, and  
343 occasionally drilled, in other sedimentary basins (Planke et al., 2000; Wright et al., 2012). Using the  
344 sequence-stratigraphic terminology applied to clinoforms, the sigmoidal reflection packages described  
345 here represent dominantly progradational sequences, indicative of transport away from areas of higher  
346 relief, with little to no aggradation (Figure 5). The relatively small height (<100 ms TWT) and  
347 progradational character of these sequences suggests that they built outwards into a shallow water  
348 environment of similar depth to the clinoform height (~100-150 m) (Figure 1b) (Patrino and Helland-  
349 Hansen, 2018; Wright et al., 2012). The presence of potential lava and/or hyaloclastite deltas, coupled  
350 with its domal geometry, suggest the Central edifice of the Tuatara Volcanic Field may have formed a  
351 shallow-water bathymetric high during its formation (Figure 3).

352 At its deepest, the base of the Central edifice lava sequence occurs within Upper Cretaceous strata  
353 (i.e. extending just below the Top Coniacian), which also onlaps onto the lowermost section of the top  
354 lava sequence (Figure 3); these observations suggest lava extrusion to form the Central edifice  
355 initiated in the Upper Cretaceous, perhaps towards the end of the Coniacian (~86 Ma). It is difficult to  
356 determine whether the edifice was constructed during a single event or through multiple, periodic  
357 extrusive phases because we cannot distinguish whether the overlapping Palaeocene and Early Eocene  
358 strata was deposited around a pre-existing dome or on a progressively growing structure. However, on  
359 some 2D seismic lines, interpreted stratigraphic horizons can seemingly be mapped into the stacked  
360 lavas sequences, and thus potentially represent syn-volcanic paleosurfaces that allow us to constrain  
361 edifice growth (Figure 3, 4). The interpreted top basement horizon continues beneath and thus  
362 predates the formation of the Central edifice (Figure 4). Whilst the top Coniacian horizon also appears  
363 to mostly continue beneath the Central edifice (Figure 4), in some areas it extends into the highly  
364 reflective lava sequences, suggesting that this interval corresponds to an early stage of Central edifice  
365 construction (Figure 3). At shallow depths, the top Early Eocene horizon blankets the edifice

366 indicating that it postdates its formation. Between these maximum and minimum age constraints, the  
367 top Paleocene horizon appears to represent the basal surface of a lava sequence in the upper parts of  
368 the high-amplitude reflection package (Figure 4), suggesting the Central edifice formed through at  
369 least two extrusive events in the Upper Cretaceous and towards the end Palaeocene.

## 370 **4.2 Mound-shaped features**

### 371 *4.2.1 Observations*

372

373 We identify a total of 69 mound-shaped features distributed atop, within, and around the Central  
374 edifice at multiple stratigraphic levels spanning the Cretaceous-to-Early Eocene (Figure 2b, 6). These  
375 mound-shaped features are characterised by a variable amplitude, typically positive polarity top  
376 surface and a sub-horizontal, conformable basal reflection (Fig. 6). Where reflections are resolved  
377 within the mounds, they are typically low- to moderate-amplitude and either parallel the top mound  
378 surface or appear sub-horizontal (Figure 5b). The majority of mounds have a prominent peak (Figure  
379 6b, e, f), although some display a flatter top (Figure 6a, c). The mounds typically have minimum  
380 heights of ~25 ms TWT and basal diameters of ~1–2 km, with the largest reaching minimum heights  
381 of up to 400 ms TWT and basal diameters of ~3 km (Figure 6).

382 The mounds are located proximal to the Central edifice, with the majority (~43) situated atop or  
383 within the high amplitude reflection package (Figure 3, 4, 7a). The top of the edifice is characterised  
384 by two large conical features surrounded by stacked lava sequences (Figure 2b, 6a). Further mounds  
385 are identified at different stratigraphic levels within the edifice itself (Figure 3, 6a). In some instances  
386 we observe that the high-amplitude reflections interpreted as lavas are often spatially related to the  
387 mounds identified here, being located around their margins and often draping atop the structures  
388 (Figure 6a, e).

389 Reflections immediately overlying the basal surface of the mound-shaped features onlap onto the  
390 flanks of the mound tops (Figure 6). Above the mound summits, reflections appear to deflect  
391 upwards, forming anticlinal folds, which occasionally host crestal faults; no reflections onlap these  
392 supra-mound folds but we note fold amplitude decays upwards (Figure 6a, d). Within one of these

393 supra-mound folds, a bright, high-amplitude, and horizontal reflection cross-cuts the folded strata  
394 (Figure 6e). In some instances, the mounds are associated with underlying vertical zones of seismic  
395 disturbance characterised relatively low-amplitudes and reflection deflection (e.g., Figure 6f).

396 To the south of the Central edifice, we identify multiple high-amplitude, positive polarity, tuned  
397 reflection packages within the Lower Eocene succession (Figure 2a, 4, 8). These high-amplitude  
398 reflections are situated beneath, but close to, the top Early Eocene horizon and are downlapped by  
399 Early Eocene-aged strata (Figure 2, 8). In places, the high-amplitude reflections appear to cross-cut  
400 and/or truncate underlying reflections (Figure 8). The amplitude of these high-amplitude reflections  
401 decreases towards a small (~300 m wide), 60 ms TWT high mound is developed (Figure 8). This  
402 central mound is underlain by a zone of chaotic and upturned stratal reflections extending downwards  
403 from ~2.4–2.7 s TWT, before transitioning into a wide (from ~1 to ~2 km) acoustically transparent  
404 zone >2.7 s TWT (Figure 8). A ~0.1 s TWT deep depression is located above the mound at the  
405 Marshall Paraconformity surface (Figure 8).

#### 406 **4.2.2 Interpretation**

407 Based on the following lines of evidence we interpret that the mound-shaped features are buried  
408 volcanoes: i) the mound-shaped geometry of the structures atop a conformable base, and the likely  
409 conical morphology of the structures in plan-view, resembles volcano geometries observed in seismic  
410 reflection data elsewhere (e.g., Jackson, 2012; Magee et al., 2013; Reynolds et al., 2018; Morley,  
411 2018) (Figure 2b; 8); ii) the positive amplitude seismic character of the mounds is consistent with a  
412 positive impedance contrast between igneous volcanic rocks and overlying sedimentary material (e.g.,  
413 Magee et al., 2015); iii) where internal structures are resolved within the mounds, the reflections  
414 parallel the top surface, consistent with volcano construction via the proportional addition of material  
415 to their summit and flanks (e.g., Magee et al., 2013); and iv) onlapping of younger strata onto the  
416 mound-shaped feature flanks, which indicates the mounds were expressed at the surface and  
417 progressively buried, thereby discounting an origin as intrusions (e.g. laccoliths) emplaced in the  
418 subsurface. The anticlines observed above some volcanoes, which are not onlapped by overlying  
419 strata (i.e. they had no surface expression) but display amplitudes that progressively decay upwards

420 (e.g., Figure 6), likely represent later differential compaction folds (e.g., Holford et al., 2017; Sun et  
421 al., 2020). Differential compaction folds may form above volcanoes because volcanic rocks (e.g.,  
422 crystalline lavas, volcanoclastics) cumulatively typically have a lower porosity than encasing and  
423 overlying, initially unconsolidated sedimentary material (e.g. Chopra and Marfurt, 2012). Upon  
424 burial, volcanoes therefore commonly compact less than the surrounding strata, promoting a  
425 differential compaction that results in the formation of anticlinal folds and associated outer-arc  
426 extension crestal faults above the volcano (e.g. Sun et al., 2020; Zhao et al., 2014), similar to those we  
427 describe here (Figure 6a, c, d).

428 The occurrence of flat tops on some volcanoes may be indicative of later erosion as they emerge at the  
429 paleo-seasurface (e.g., Bischoff et al., 2019; Bischoff et al., 2017), or may simply be a product of the  
430 volcano being intersected along its flank (not across its centre) by the 2D seismic lines. Sub-  
431 horizontal reflections within volcanoes may also correspond to the cut-effect of the seismic line  
432 sampling the flank of the structure. Although we are unable to determine the eruptive history of  
433 individual volcanoes, the distribution of multiple, relatively small volcanoes within a relatively  
434 localised area (typically 20-30 km from the centre of the Central edifice), suggests that they may  
435 represent a monogenetic volcanic field (Németh, 2010; Németh and White, 2003). Geometrically, the  
436 distribution of volcanoes bears similarities to that of the monogenetic Auckland Volcanic Field in the  
437 North Island (Cassidy and Locke, 2010; Le Corvec et al., 2013; Rout et al., 1993; Spörli and  
438 Eastwood, 1997), as well as monogenetic volcanic fields identified in seismic reflection data  
439 elsewhere (Bischoff et al., 2020; Bischoff et al., 2019; McLean et al., 2017).

440 Due to their clustering within and surrounding the Central edifice, we suggest that, at least for the  
441 upper parts of the domal edifice, the volcanoes may have been responsible for the eruption of the  
442 stacked lava packages, with the majority of activity occurring in the Paleocene. The volcanoes are  
443 located at different stratigraphic levels within the reflection package, with buried cones likely  
444 responsible for the eruption of older lavas (Figure 3, 6a). Additional volcanoes, and potential fissure  
445 vents, may be present at greater depths beneath the edifice although we are unable to resolve these  
446 structures due to a lack of imaging beneath the thick lava sequence (Quirie et al., 2019) (Figure 3).

447 To the south of the Central edifice, we interpret the small mound as a small, Early Eocene-aged  
448 volcano, with the adjacent high amplitude reflections interpreted as associated lava flows (Figure 8).  
449 This interpretation is corroborated by zone of chaotic and washed out reflectivity beneath the structure  
450 and the immediately adjacent upturned strata (Figure 8). The upturned strata are interpreted as a  
451 velocity pull-up, a seismic artefact generated due to relatively high velocities beneath the structure,  
452 suggestive of igneous material. The sub-vertical chaotic reflectivity beneath the volcano may  
453 correspond to igneous dykes or pipes, forming a vertical plumbing system to individual volcanoes  
454 (Figure 6f, 8) (Wall et al., 2010). The apparent small size of this cone may be a result of the seismic  
455 section only intersecting the margin of the structure, rather than passing through its centre (Figure 8).  
456 The volcano is associated with a series of Early Eocene high-amplitude reflections, which we interpret  
457 as erupted lava flows (Figure 8). The brightening of the lava flows away from the volcanic cone likely  
458 represents a decrease in thickness, and an associated increase in seismic tuning, towards their  
459 termination (Kallweit and Wood, 1982; Smallwood and Maresh, 2002; Widess, 1973) (Figure 8). The  
460 truncation of underlying strata by the lava flows may correspond to the formation of lava channels  
461 and the associated bulldozing and erosion of the underlying stratigraphy (Sun et al., 2019a). The  
462 onlapping of Early Eocene strata onto the lava flow may relate to the dominantly contouritic nature of  
463 the stratigraphy in this interval (Figure 1b). The depression on the Marshall Paraconformity surface  
464 co-located above the Early Eocene volcano cone appears to have formed due to fluid expulsion  
465 following burial of the volcano, which focussed migrating, non-volcanic-related fluids (Figure 8)  
466 (Holford et al., 2017; Sun et al., 2020). Buried volcanoes elsewhere have been shown to act as  
467 conduits for later fluid flow in the subsurface (Holford et al., 2017; Sun et al., 2020). We also interpret  
468 the sub-horizontal, high-amplitude reflection within the overlying differential compaction fold of one  
469 volcano as a ‘flat-spot’, likely corresponding to a trapped gas pocket (Figure 6e).

## 470 **4.3 High-amplitude transgressive reflections**

### 471 ***4.3.1 Observations***

472



473 Aside from the high-amplitude, sub-horizontal reflection packages interpreted as lava flows, we  
474 identify 92 high-amplitude, positive polarity reflections that are laterally discontinuous and commonly  
475 display transgressive, saucer-shaped or inclined morphologies (Figure 9). These features typically  
476 have lengths ranging from 1-3 km, individually span depth ranges up to ~0.2 s TWT, and are  
477 observed at different stratigraphic levels between the pre-Coniacian and the Paleocene (Figure 7b, 9).  
478 Many of these transgressive high-amplitude reflections are located beneath interpreted volcanoes,  
479 although some appear independent of extrusive features and occur up to 30-40 km from the Central  
480 edifice (Figure 7b). The majority of these high-amplitude transgressive reflections are associated with  
481 clear anticlinal folds in the overlying strata, the outer inflection points of which directly overlie the  
482 lateral terminations of the high-amplitude reflection (Figure 9). These folds can be identified  
483 throughout Late Cretaceous-to-Early Eocene strata, with strata onlapping onto their margins (Figure  
484 9).

#### 485 ***4.3.2 Interpretation***

486 We interpret these high-amplitude, transgressive reflections as igneous sills because: i) the high  
487 amplitude and positive reflection that defines their upper surface is consistent with an acoustically  
488 hard lithology, such as igneous material (Hansen et al., 2008); ii) they transgress and cross-cut  
489 background reflections, distinguishing these feature from the aforementioned lava flows, but do not  
490 offset strata and thus are not faults; and iii) their typical saucer-shaped geometry is similar to sheet  
491 intrusions identified onshore (Galerie et al., 2011; Ledevin et al., 2012; Polteau et al., 2008) and  
492 igneous sills resolved in seismic data, some of which have been drilled, from the Rockall Basin  
493 (Morewood et al., 2004; Thomson and Hutton, 2004), Faroe-Shetland Basin (McLean et al., 2017;  
494 Smallwood and Maresh, 2002), offshore Australia (Jackson, 2012; Magee et al., 2017; Magee et al.,  
495 2016), and in the Canterbury Basin offshore New Zealand (Bischoff et al., 2017; Reeves et al., 2018).  
496 We are able to relate the 92 high-amplitude features identified here as corresponding to ~79 individual  
497 sills, with some sills resolved across multiple seismic sections. Additional sills may be present  
498 beneath the main central dome, but they are not resolved in our data (Figure 3, 4, 7b). Overall, we  
499 classify the mapped intrusions as a sill-complex (Magee et al. 2016).

500 We interpret the folds overlying some of the sills as intrusion-induced forced folds that formed via  
501 overburden uplift to accommodate shallow-level magma emplacement (Hansen and Cartwright, 2006;  
502 Magee et al., 2013a; Reeves et al., 2018; Trude et al., 2003). Recognition of overlying strata  
503 onlapping onto these folds indicates the top fold surface corresponded to the syn-emplacement  
504 palaeosurface (Figure 9), and can be used to date intrusion (e.g. Trude et al., 2003). For those sills not  
505 overlain by forced folds we use the age of the encasing strata as a maximum estimate for  
506 emplacement timing; i.e. whilst ascending magma may arrest to form sills at any stratigraphic or  
507 structural level, in response to a range of different mechanisms (e.g., Kavanagh et al., 2006; Magee et  
508 al., 2016; Menand, 2011), its emplacement has to be younger than the host material age. We  
509 acknowledge that simply using host rock age to establish relative emplacement timings is not ideal  
510 because the mapped sills could be significantly younger than the rocks they intruded. Regardless,  
511 based on our defined maximum ages for sill emplacement and the seismic-stratigraphic onlap  
512 relationships, which allow to us accurately constrain emplacement age (e.g., Trude et al., 2003), we  
513 estimate sills ages within the Tuatara Volcanic Field range from the pre-Santonian (Top Teratan -  
514 >86.3 Ma) to Early Eocene (Top Heretaungan – 45.7 Ma), representing over 40 Myr of magmatic  
515 activity.

516

## 517 **5 Distribution and age of volcano-magmatic structures in the**

### 518 **Tuatara Volcanic Field**

519 The Central edifice of the Tuatara Volcanic Field, which comprises stacked lava sequences,  
520 hyaloclastites, and volcanoes covers a ~270 km<sup>2</sup> elliptical area that is elongated in a NW-SE  
521 orientation (Figure 2); this part of the Tuatara Volcanic Field has been referred to as the Tapuku East  
522 volcanics (Bischoff et al., preprint). Igneous sills are much more widely distributed around the Central  
523 edifice than the volcanoes (Figure 7b). A subtle WNW-ESE trend is present in the spatial distribution  
524 of volcanoes and sills; this is more pronounced with the volcanoes (Figure 7). By determining the age  
525 of emplacement for the sills and volcanic cones, we assign these structures to stratigraphic intervals  
526 and examine how their distribution evolved temporally. Those volcanoes and sills emplaced prior to

527 the Santonian (>86.3 Ma) are typically located ~30 km to the southeast of the Central edifice, with  
528 some pre-Santonian aged sills also present northeast of the Central edifice (Figure 7). Late Cretaceous  
529 sills (from 86.3-66 Ma) are located closer to the Central edifice (~20 km) but distributed around its  
530 SW, SE, and NE sides (Figure 7b). No Late Cretaceous volcanoes were identified. Paleocene-aged  
531 structures are the most abundant across the area. Paleocene-aged volcanoes are relatively tightly  
532 clustered around the central dome compared to older volcanoes (~10 km) (Figure 7a). Paleocene sills  
533 are more proximal to the Central edifice relative to older sills, although they are still relatively  
534 distributed compared to volcanoes of the same age (Figure 7b). A cluster of Paleocene sills occur  
535 immediately west-northwest of the central dome. Early Eocene and younger sills and volcanoes occur  
536 to the northwest of the main edifice, with the exception of one sill straddling the Paleocene-Eocene  
537 boundary (Figure 9d), suggesting a broad north-westward migration of igneous activity from the pre-  
538 Santonian to the Early Eocene (Figure 7). The youngest structures, an Early Eocene sill (56-45.7 Ma)  
539 and a volcanoes younger than the Early Eocene (<45.7 Ma) (Figure 6b), are both located ~25-30 km  
540 to the northwest of the Central edifice, whereas the oldest interpreted structures are located  
541 approximately ~35 km to the southeast (Figure 7). Based on their overall clustering and age  
542 progression centred on the Central edifice we interpret the younger intrusions form part of the same  
543 volcanic system, focussed by the same mechanism as the older structures, as opposed to being part of  
544 an unrelated, later magmatic event (Bischoff et al., preprint).

545 The size, connectivity, and cumulative volume of the resolved sill-complex we map does not take into  
546 account the likely presence of thin sills, with thicknesses below the limits of visibility of the data (i.e.  
547  $\leq 7$  m), which are difficult to identify in seismic reflection data (e.g., Eide et al., 2018; Schofield et  
548 al., 2017). Given that there are likely more sills present in the area than are resolved and that the  
549 mapped volcanoes and sills display a similar spatial and temporal distribution (Figure 7), with some  
550 intrusions seemingly extending up to the base of some volcanic edifices (e.g., Figure 6c), we suggest  
551 the sill-complex likely played a role in delivering magma to the surface. Inferring that the mapped  
552 sill-complex likely fed parts the Tuatara Volcanic Field implies some individual volcanoes may have  
553 been connected; i.e. activity at one volcano could have been linked to eruption at another as they

554 probably shared a plumbing system (Magee et al., 2016). We acknowledge that dykes or magma  
555 conduits that have since closed may be or have been present across the study area respectively, and  
556 probably contributed to the magma plumbing system. However, the expected sub-vertical geometry  
557 and thin nature of dykes, as well as that of closed conduits and associated remnant host rock changes  
558 (e.g. thermal aureoles), means that these structures are difficult to resolve on seismic reflection data  
559 (see Magee and Jackson, 2020 and references therein). Some volcanoes within the Tuatara Volcanic  
560 Field do appear to be underlain by pronounced vertical seismic disturbances, which we tentatively  
561 interpret as corresponding to dykes (Figure 6f, 7) (e.g., Magee and Jackson, 2020; Wall et al., 2010).  
562 In particular, these inferred dykes are largely resolved beneath, and appear to feed, isolated volcanic  
563 cones away from the central edifice (Figure 7a).

564

## 565 **6 Discussion**

566 The Tuatara Volcanic Field occupies a relatively localised (~270 km<sup>2</sup>) setting above the Livingstone  
567 Fault, which marks the boundary between the Dun Mountain-Maitai Terrane to the south, and the  
568 Caples Terrane in the north (Figure 10) (Mortimer et al., 2002; Tarling et al., 2019). Here, we  
569 examine the controls on the localisation, geometry, and longevity of intraplate volcanic activity at the  
570 Tuatara Volcanic Field. We also discuss how our observations of the internal structure and plumbing  
571 system of the Tuatara Volcanic Field may relate to the Auckland Volcanic Field and enhance our  
572 understanding of intraplate volcanic systems generally.

### 573 **6.1 Controls on the location of the Tuatara Volcanic Field**

574 Intraplate volcanism appears to display a relatively random distribution across Zealandia (Bischoff et  
575 al., preprint; Hoernle et al., 2006; Timm et al., 2010); similar areas of diffuse intraplate volcanism  
576 have been identified across the Turkish-Iranian Plateau (Kaislaniemi et al., 2014). Such diffuse  
577 regions of intraplate volcanism have been related to decompression melting of upwelling  
578 asthenosphere into areas where Rayleigh-Taylor instabilities and/or small-scale mantle convection,  
579 which occur due to density contrasts at the lithosphere-asthenosphere boundary and/or hydrated

580 mantle following protracted subduction, has detached lithospheric material (Elkins-Tanton, 2005;  
581 Hoernle et al., 2006; Kaislaniemi et al., 2014). According to these models, intraplate volcanic systems  
582 are located directly above the seemingly randomly distributed areas of detaching lithosphere and  
583 associated decompression melting (Elkins-Tanton, 2005; Hoernle et al., 2006; Kaislaniemi et al.,  
584 2014). However, because some volcanic systems, such as those on the Chatham Islands and Banks  
585 Peninsula, display repeated phases of activity with long intervening periods (Figure 1) (Hoernle et al.,  
586 2006; Timm et al., 2009), it is necessary to consider how localised areas of lithospheric detachment  
587 and volcanic activity could be rejuvenated.

588 We consider lithospheric detachment as the likely mechanism for activity at the Tuatara Volcanic  
589 Field, which we suggest is reflected in its elliptical geometry, similar to that of the Auckland Volcanic  
590 Field; i.e. the areal extent of the Tuatara Volcanic Field likely marks the limits of an underlying zone  
591 of melt where the lithosphere detached (Le Corvec et al., 2013; Spörli and Eastwood, 1997).  
592 However, we also note that the Tuatara Volcanic Field overlies the Livingstone Fault, which marks  
593 the boundary between the Caples and Dun Matai terranes. The Auckland Volcanic Field and  
594 volcanoes on the Banks Peninsula are also co-located along prominent basement terrane boundaries,  
595 namely the same boundary as the Tuatara Volcanic Field, between the Dun Mountain-Maitai and  
596 Caples terranes, and the Rakaia and Pahau terranes respectively (Figure 1a) (Eccles et al., 2005;  
597 Mortimer et al., 2002; Tarling et al., 2019). This co-location of volcanic fields with major basement  
598 terrane boundaries questions whether the localisation of intraplate volcanic systems may, at least  
599 partially, be controlled by pre-existing structures. For example, faults have been shown to act as  
600 conduits for magma and may thus spatially correlate with the plumbing systems of volcanoes (e.g.  
601 Mazzarini, 2007). Based on the overall location of the Tuatara Volcanic Field and the approximate  
602 NW-alignment of constituent volcanoes and sills, parallel to the underlying basement terranes and  
603 Livingstone Fault (Figure 2b), we suggest that the location of the Tuatara Volcanic Field was  
604 primarily controlled by underlying pre-existing structures. In particular, we envisage that the  
605 Livingstone Fault, and perhaps sub-vertical foliations within the Dun Mountain-Matai terrane,

606 provided viable pathways for magma ascending through the crust (Eccles et al., 2005; Hopkins et al.,  
607 2020).

608 Considering the location of the Tuatara Volcanic Field is linked to that of the Livingstone Fault at  
609 upper crustal depths, we in turn question whether the site of lithosphere detachment could have been  
610 influenced by pre-existing structures. Regional seismic reflection data located offshore of the South  
611 Island indicate that the Livingstone Fault extends down to at least the Moho (Figure 1, 10c) (Mortimer  
612 et al., 2002). If the Dun Mountain-Matai and Caples terranes, which accreted to the southern margin  
613 of Gondwana, are characterised by different lithospheric thicknesses and properties, we suggest that  
614 the Livingstone Fault could extend deeper and have some expression at the base of the lithosphere  
615 (i.e. a change in lithospheric thickness or narrow keel; Figure 10c) (Eccles et al., 2005; Tarling et al.,  
616 2019). Such promontories at the base of the lithosphere may provide a first-order control on the  
617 development of small-scale mantle convection cells and Rayleigh-Taylor instabilities, focussing the  
618 detachment of lithospheric material (Figure 10c). Elsewhere, small-scale convection cells will be  
619 controlled by the spacing between adjacent cells, causing lithosphere detachment and the associated  
620 intraplate volcanic systems to not be ‘directly’ related to a pre-existing structure and appear randomly  
621 distributed (Kaislaniemi et al., 2014). Therefore, whilst pre-existing structures appear to control, or at  
622 least influence, the location of some individual intraplate volcanic systems (e.g., the Tuatara Volcanic  
623 Field), it also allows for a random background distribution of intraplate volcanic systems that bear no  
624 apparent relation to pre-existing structure.

625 Although spatial correlation suggests the location of the Tuatara Volcanic Field as a whole was  
626 influenced by pre-existing structures, it is difficult to ascertain whether its individual intrusive or  
627 extrusive components were similarly structurally controlled. For example, at shallow depths within  
628 the Tuatara Volcanic Field, we are unable to fully constrain the geometry of rift-related faults beneath  
629 the Central edifice, although faults typically strike NE-SW across the Great South and Canterbury  
630 Basins (Phillips and McCaffrey, 2019; Uruski et al., 2007; Uruski, 2010). Overall, we suggest the  
631 transition from vertical magma ascent from the base of the lithosphere, likely via dykes, to apparently  
632 favour the formation of a sill-complex within the Great South Basin may have been related to a local

633 change in the differential stress field at shallower depths (Stephens et al., 2017), and/or deflection of  
634 magma pathways along sub-horizontal boundaries (Kavanagh et al., 2006; Kenny et al., 2012).

## 635 **6.2 Controls on the longevity of the Tuatara Volcanic Field**

636 The longevity of intraplate volcanic systems across Zealandia (i.e. those not related to rift activity) is  
637 proposed to be determined by the time taken for the area of material detached from the base of the  
638 lithosphere to anneal, thereby stopping any decompression melting of upwelling asthenosphere  
639 (Timm et al., 2009). Accordingly, the larger the diameter and depth of the volume of detached  
640 lithosphere, the greater the expected magmatism, either in magnitude or longevity. The magnitude of  
641 melting in turn influences the resultant style of volcanism; low-Si monogenetic volcanic fields are  
642 thought to relate to small areas of detaching lithosphere producing small-degree melts with larger  
643 shield volcanoes (i.e. those at Banks Peninsula) associated with larger and deeper areas of detaching  
644 lithosphere producing larger-degrees of melting (Hoernle et al., 2006).

645 We document a ~40 Myr record of magmatic and volcanic activity across the Tuatara Volcanic Field  
646 lasting from ~85–45 Ma. Earlier volcano-magmatic features may be present at deeper levels, although  
647 we are unable to resolve structures at these depths (Figure 3, 4). The earliest phases of activity in the  
648 Tuatara Volcanic Field appear to post-date the cessation of subduction along the southern margin of  
649 Gondwana caused by impingement of the Hikurangi Plateau (Davy et al., 2008), and overlap with  
650 rifting associated with Gondwana breakup, which lasted until ~80 Ma (Kula et al., 2007; Tulloch et  
651 al., 2019). The vast majority of volcano-magmatic activity in the Tuatara Volcanic Field and across  
652 Zealandia occurred in an intraplate setting, with the main period of activity during the Paleocene  
653 (Figure 10a).

654 The ages of sills and volcanoes identified within the Tuatara Volcanic Field migrates towards the  
655 northwest through time, following the orientation of the underlying basement terranes (Figure 7).  
656 Similarly, at the Banks Peninsula on the South Island, volcanic activity migrates along the NW-  
657 trending boundary between the Pahau and Rakaia terranes, albeit migrating in the opposite direction  
658 to that observed at the Tuatara Volcanic Field. Volcanic activity initially occurs at the Lyttelton

659 Volcano in the northwest (12.3-10.4 Ma), before migrating to the Akaroa Volcano ~25 km southeast  
660 (9.4-6.8 Ma), correlating to the NW-trending terrane boundary between the Pahau and Rakaia  
661 terranes, (Timm et al., 2009). In the case of Banks Peninsula, this may reflect progressive lithosphere  
662 detachment towards the southeast along the terrane boundary; as the lithosphere begins to anneal  
663 beneath the Lyttelton Volcano, further detachment occurs to the southeast leading to activity at the  
664 Akaroa Volcano (Timm et al., 2009). We propose a similar mechanism of along-strike progressive  
665 lithospheric detachment focused along the expression of the Livingstone Fault at the lithosphere-  
666 asthenosphere boundary to explain the longevity and age progression within the Tuatara Volcanic  
667 Field (Figure 11) (Mortimer, 2004). In particular, we suggest such localisation by pre-existing  
668 structures may result in a quasi-periodic ‘dripping’ of material from the base of the lithosphere,  
669 focussing magmatic upwelling and inhibiting the complete annealing of the lithosphere over  
670 prolonged (>10 Myr) periods. That monogenetic volcanic fields are typically characterised by small-  
671 degree melts (Hoernle et al., 2006; Timm et al., 2009) suggests this quasi-periodic dripping is  
672 involves relatively small, but relatively frequent detaching of lithospheric material.

### 673 **6.3 Implications for intraplate volcanism**

674 We document the 3D geometry and longevity of an intraplate volcanic system, highlighting that  
675 seismic reflection data can potentially provide important insights into the processes driving intraplate  
676 volcanism. To explore the applicability of our findings to other examples of intraplate volcanism  
677 across New Zealand, we here compare to similar volcanic fields occur in the same structural setting  
678 on the North Island, where basement terranes are offset along the Alpine Fault (Figure 1a). There is a  
679 northwards younging of volcanic fields along the Dun Mountain ophiolite belt in the North Island;  
680 from the Okete volcanic field in the south (2.69–1.8Ma), northwards to the Ngatutura (1.83–1.54Ma),  
681 South Auckland (1.59–0.51Ma), and the recently active Auckland Volcanic Field (193 Ka–500 yr BP)  
682 (Hopkins et al., 2020). In particular, we find that, the recently active (last eruption 500 yr before  
683 present) Auckland Volcanic Field on the North Island is situated in the same structural setting, i.e.  
684 above the terrane boundary between the Dun-Mountain-Maitai and Caples terranes represented by the  
685 Livingstone Fault, as the Tuatara Volcanic Field on the opposite side of the Alpine Fault on the South



686 Island (Figure 1a, 10b) (e.g. Cassidy and Locke, 2010; Lindsay et al., 2011; McGee et al., 2013; Rout  
687 et al., 1993; Spörli et al., 2015; Tarling et al., 2019). Both volcanic fields display similar geometric  
688 characteristics at the surface: the Auckland Volcanic Field is characterised by ~50 individual volcanic  
689 centres (each typically ~1–2 km in diameter) distributed across a roughly elliptical area with a ~29 km  
690 long axis and a short axis of ~16 km (~375 km<sup>2</sup>) (Hopkins et al., 2020; Le Corvec et al., 2013;  
691 Lindsay et al., 2011; Spörli and Eastwood, 1997); this is compared to 69 volcanoes (typically 1–2 km  
692 in diameter) identified within the 23 km x 15 km (~270 km<sup>2</sup>) Tuatara Volcanic Field. The Tuatara  
693 Volcanic Field may thus represent a crucial ancient analogue to the Auckland Volcanic Field,  
694 potentially helping to constrain our understanding of the currently uncertain magma plumbing system  
695 and subsurface geology of the latter. In particular, the shallow-level plumbing system of the Tuatara  
696 Volcanic Field involves interconnected sills (Figure 6f). If the Auckland Volcanic Field also  
697 comprises a shallow-level, sill-complex, in addition to dykes, it is plausible that individual volcanoes  
698 could be linked such that (Magee et al., 2016): (i) activity at one could instigate activity at another;  
699 and/or (ii) pre-eruption warning signals (e.g., ground deformation and seismicity) may be laterally  
700 offset from the subsequent eruption site. Our work also implies that extinct volcanoes may be buried  
701 beneath the current exposure of the Auckland Volcanic Field; these buried volcanoes could provide  
702 pathways for fluid/gas escape (e.g., Figure 6b) (e.g., Holford et al., 2017; Sun et al., 2020). Finally,  
703 whilst we are unable to directly comment on the likely longevity of volcanic activity in the Auckland  
704 Volcanic Field, observations from the Tuatara Field described here suggest that volcanic fields partly  
705 controlled by pre-existing structures could periodically be rejuvenated. Overall, hazard assessment of  
706 the Auckland Volcanic Field should take into account potential constraints on the location, geometry,  
707 and longevity of the system afforded by our study of the analogue Tuatara Volcanic Field.

708

## 709 **7 Conclusions**

710 We use seismic reflection data to image and document a newly discovered volcanic field, which we  
711 name the Tuatara Volcanic Field, located in the Great South Basin, offshore of the South Island of

712 New Zealand. The ~270 km<sup>2</sup> Tuatara Volcanic Field is characterised by a central edifice comprising  
713 stacked lava and hyaloclastite sequences surrounded by 69 volcanoes connected by a sill-complex; we  
714 consider dykes also play an important role in the plumbing system but these are not imaged in our  
715 data. Igneous activity occurred periodically over 40 Myr, beginning after rifting in the Late  
716 Cretaceous (~85 Ma) and continuing until the Early-to-Mid Eocene (~45 Ma). The Tuatara Volcanic  
717 Field thus represents one of the longest-lived volcanic systems in Zealandia and potentially elsewhere.  
718 The location of the Tuatara Volcanic Field coincides with the Livingstone Fault, a crustal-to-  
719 lithosphere scale boundary between the Dun Mountain-Maitai and Caples terranes, which we suggest  
720 facilitated magma ascent. Activity within the field migrates towards the northwest and to higher  
721 stratigraphic levels through time, following the orientation of the underlying basement structure. We  
722 suggest that the Livingstone Fault had some expression at the base of the lithosphere, which  
723 periodically promoted detachment of material from the lithosphere by Rayleigh-Taylor instabilities  
724 and/or small-scale mantle convection. Decompression melting of upwelling asthenosphere into this  
725 area of detached lithosphere likely controlled the site of the Tuatara Volcanic Field. Where such pre-  
726 existing structures are absent, lithosphere detachment and intraplate volcanism may occur randomly  
727 and display shorter periods of activity.

728 The geometry and structural setting of the Tuatara Volcanic Field resembles the Auckland Volcanic  
729 Field; the locations of both volcanic fields appear to be controlled by the pre-existing Livingstone  
730 Fault and terrane boundary. We suggest that the Tuatara Volcanic Field represents an ancient  
731 analogue to the Auckland Volcanic Field. Our observations of the internal structure and longevity of  
732 the Tuatara Volcanic Field may thus provide important insight into potential future activity at the  
733 Auckland Volcanic Field. In particular, whilst magma transport is dominantly vertical throughout the  
734 lithosphere, the plumbing system of the Auckland Volcanic Field may include a sill-complex that  
735 could connect and control the distribution of volcanoes within the field. Furthermore, we postulate  
736 that the longevity and progression of activity at the Tuatara Volcanic Field could imply that the  
737 Auckland Volcanic Field is perhaps relatively early in its evolution and that activity may migrate  
738 along the pre-existing structure across geological time. In this study, we have characterised the

739 internal plumbing system of a volcanic system offshore New Zealand. We highlight how pre-existing  
740 crustal and lithospheric structure exert an important influence over the location and longevity of  
741 individual intraplate volcanic systems. We offer insights into the internal structure and plumbing  
742 system of these volcanic fields that may be applicable to other ancient and active intraplate systems.

## 743 **Acknowledgements**

744 The authors would like to thank the Leverhulme Trust for funding an Early Career Fellowship for  
745 Phillips. Magee is funded by a NERC independent research fellowship. The authors would also like to  
746 thank New Zealand Petroleum and Minerals for making the seismic reflection data used in this study  
747 publically available, and Schlumberger for providing access to academic licences for Petrel software.  
748 We also thank Francesco Mazzarini and an anonymous reviewer for reviewing the manuscript, and  
749 Tyrone Rooney for editorial handling.

750

## 751 **Funding**

752 This project is funded by a Leverhulme Early Career Fellowship provided to Phillips at the University  
753 of Durham.

754

755

## 756 **References**

757 Acocella, V., Spinks, K., Cole, J., Nicol, A., 2003. Oblique back arc rifting of Taupo  
758 Volcanic Zone, New Zealand. *Tectonics* 22.

759 Adams, C.J., 1983. Age of the volcanoes and granite basement of the Auckland Islands,  
760 Southwest Pacific. *New Zealand Journal of Geology and Geophysics* 26, 227-237.

761 Adams, R.D., 1962. Thickness of the earth's crust beneath the Campbell Plateau. *New*  
762 *Zealand Journal of Geology and Geophysics* 5, 74-85.

763 Beggs, J., 1993. Depositional and tectonic history of the Great South Basin. *South Pacific*  
764 *sedimentary basins. Sedimentary basins of the World* 2, 365-373.

- 765 Bertonni, C., Gan, Y., Paganoni, M., Mayer, J., Cartwright, J., Martin, J., Van Rensbergen, P.,  
766 Wunderlich, A., Clare, A., 2019. Late Paleocene pipe swarm in the Great South – Canterbury  
767 Basin (New Zealand). *Marine and Petroleum Geology* 107, 451-466.
- 768 Bischoff, A., Barrier, A., Beggs, M., Nicol, A., Cole, J., Sahoo, T., Preprint. Magmatic and  
769 Tectonic Interactions in Te Riu-a-Māui/Zealandia Sedimentary Basins.  
770 10.13140/RG.2.2.33641.24166
- 771 Bischoff, A., Nicol, A., Barrier, A., Wang, H., 2020. Characterization of a Middle Miocene  
772 Monogenetic Volcanic Field Buried in the Canterbury Basin, New Zealand – Part II.
- 773 Bischoff, A., Nicol, A., Rossetti, M., Kennedy, B., 2019. Characterization of a Middle  
774 Miocene Monogenetic Volcanic Field Buried in the Canterbury Basin, New Zealand – Part I.  
775 EarthArXiv.
- 776 Bischoff, A.P., Nicol, A., Beggs, M., 2017. Stratigraphy of architectural elements in a buried  
777 volcanic system and implications for hydrocarbon exploration. *Interpretation* 5, SK141-  
778 SK159.
- 779 Bishop, D., Bradshaw, J., Landis, C., 1985. Provisional terrane map of South Island, New  
780 Zealand.
- 781 Brown, A.R., 2011. Interpretation of three-dimensional seismic data. *Society of Exploration  
782 Geophysicists and American Association of Petroleum ...*
- 783 Buntin, S., Malehmir, A., Koyi, H., Högdahl, K., Malinowski, M., Larsson, S.Å., Thybo, H.,  
784 Juhlin, C., Korja, A., Górszczyk, A., 2019. Emplacement and 3D geometry of crustal-scale  
785 saucer-shaped intrusions in the Fennoscandian Shield. *Scientific Reports* 9, 10498.
- 786 Calvès, G., Schwab, A.M., Huuse, M., Clift, P.D., Gaina, C., Jolley, D., Tabrez, A.R., Inam,  
787 A., 2011. Seismic volcanostratigraphy of the western Indian rifted margin: The pre-Deccan  
788 igneous province. *Journal of Geophysical Research: Solid Earth* 116.
- 789 Cassidy, J., Locke, C.A., 2010. The Auckland volcanic field, New Zealand: Geophysical  
790 evidence for structural and spatio-temporal relationships. *Journal of Volcanology and  
791 Geothermal Research* 195, 127-137.
- 792 Chenrai, P., Huuse, M., 2020. Sand injection and polygonal faulting in the Great South Basin,  
793 New Zealand. *Geological Society, London, Special Publications* 493, SP493-2018-2107.
- 794 Chopra, S., Marfurt, K.J., 2012. Seismic attribute expression of differential compaction. *The  
795 Leading Edge* 31, 1418-1422.
- 796 Clague, D.A., Jarrard, R.D., 1973. Tertiary Pacific Plate Motion Deduced from the Hawaiian-  
797 Emperor Chain. *GSA Bulletin* 84, 1135-1154.

- 798 Clouard, V., Bonneville, A., 2005. Ages of seamounts, islands, and plateaus on the Pacific  
799 plate. *Special Papers-Geological Society of America* 388, 71.
- 800 Collanega, L., Jackson, C.A.L., Bell, R.E., Coleman, A.J., Lenhart, A., Breda, A., 2018.  
801 Normal fault growth influenced by basement fabrics: the importance of preferential  
802 nucleation from pre-existing structures. *Basin Res* 0.
- 803 Cooper, A.F., Barreiro, B.A., Kimbrough, D.L., Mattinson, J.M., 1987. Lamprophyre dike  
804 intrusion and the age of the Alpine fault, New Zealand. *Geology* 15, 941-944.
- 805 Cooper, A.F., Norris, R.J., 1994. Anatomy, structural evolution, and slip rate of a plate-  
806 boundary thrust: The Alpine fault at Gaunt Creek, Westland, New Zealand. *GSA Bulletin*  
807 106, 627-633.
- 808 Davey, F.J., Christoffel, D.A., 1978. Magnetic anomalies across Campbell Plateau, New  
809 Zealand. *Earth and Planetary Science Letters* 41, 14-20.
- 810 Davies, D.R., Rawlinson, N., Iaffaldano, G., Campbell, I.H., 2015. Lithospheric controls on  
811 magma composition along Earth's longest continental hotspot track. *Nature* 525, 511.
- 812 Davy, B., Hoernle, K., Werner, R., 2008. Hikurangi Plateau: Crustal structure, rifted  
813 formation, and Gondwana subduction history. *Geochemistry, Geophysics, Geosystems* 9.
- 814 Eccles, J.D., Cassidy, J., Locke, C.A., Spörli, K.B., 2005. Aeromagnetic imaging of the Dun  
815 Mountain Ophiolite Belt in northern New Zealand: insight into the fine structure of a major  
816 SW Pacific terrane suture. *Journal of the Geological Society* 162, 723.
- 817 Eide, C.H., Schofield, N., Lecomte, I., Buckley, S.J., Howell, J.A., 2018. Seismic  
818 interpretation of sill complexes in sedimentary basins: implications for the sub-sill imaging  
819 problem. *Journal of the Geological Society* 175, 193-209.
- 820 Elkins-Tanton, L.T., 2005. Continental magmatism caused by lithospheric delamination, in:  
821 Foulger, G.R., Natland, J.H., Presnall, D.C., Anderson, D.L. (Eds.), *Plates, plumes and*  
822 *paradigms*. Geological Society of America, p. 0.
- 823 Finn, C.A., Müller, R.D., Panter, K.S., 2005. A Cenozoic diffuse alkaline magmatic province  
824 (DAMP) in the southwest Pacific without rift or plume origin. *Geochemistry, Geophysics,*  
825 *Geosystems* 6.
- 826 Fulthorpe, C.S., Carter, R.M., Miller, K.G., Wilson, J., 1996. Marshall Paraconformity: a  
827 mid-Oligocene record of inception of the Antarctic circumpolar current and coeval glacio-  
828 eustatic lowstand? *Marine and Petroleum Geology* 13, 61-77.
- 829 Galerne, C.Y., Galland, O., Neumann, E.-R., Planke, S., 2011. 3D relationships between sills  
830 and their feeders: evidence from the Golden Valley Sill Complex (Karoo Basin) and  
831 experimental modelling. *Journal of Volcanology and Geothermal Research* 202, 189-199.

- 832 Gallagher, J.W., Dromgoole, P.W., 2007. Exploring below the basalt, offshore Faroes: a case  
833 history of sub-basalt imaging. *Petroleum Geoscience* 13, 213.
- 834 Grindley, G.W., Adams, C.J.D., Lumb, J.T., Watters, W.A., 1977. Paleomagnetism, K-Ar  
835 dating and tectonic interpretation of Upper Cretaceous and Cenozoic volcanic rocks of the  
836 Chatham Islands, New Zealand. *New Zealand Journal of Geology and Geophysics* 20, 425-  
837 467.
- 838 Grobys, J.W.G., Gohl, K., Uenzelmann-Neben, G., Davy, B., Barker, D., 2009. Extensional  
839 and magmatic nature of the Campbell Plateau and Great South Basin from deep crustal  
840 studies. *Tectonophysics* 472, 213-225.
- 841 Hansen, D.M., Cartwright, J., 2006. The three-dimensional geometry and growth of forced  
842 folds above saucer-shaped igneous sills. *Journal of Structural Geology* 28, 1520-1535.
- 843 Hansen, D.M., Redfern, J., Federici, F., di Biase, D., Bertozzi, G., 2008. Miocene igneous  
844 activity in the Northern Subbasin, offshore Senegal, NW Africa. *Marine and Petroleum  
845 Geology* 25, 1-15.
- 846 Higgs, K.E., Browne, G.H., Sahoo, T.R., 2019. Reservoir characterisation of syn-rift and  
847 post-rift sandstones in frontier basins: An example from the Cretaceous of Canterbury and  
848 Great South basins, New Zealand. *Marine and Petroleum Geology* 101, 1-29.
- 849 Hoernle, K., White, J.D.L., van den Bogaard, P., Hauff, F., Coombs, D.S., Werner, R., Timm,  
850 C., Garbe-Schönberg, D., Reay, A., Cooper, A.F., 2006. Cenozoic intraplate volcanism on  
851 New Zealand: Upwelling induced by lithospheric removal. *Earth and Planetary Science  
852 Letters* 248, 350-367.
- 853 Holford, S.P., Schofield, N., Reynolds, P., 2017. Subsurface fluid flow focused by buried  
854 volcanoes in sedimentary basins: Evidence from 3D seismic data, Bass Basin, offshore  
855 southeastern Australia. *Interpretation* 5, SK39-SK50.
- 856 Hopkins, J.L., Smid, E.R., Eccles, J.D., Hayes, J.L., Hayward, B.W., McGee, L.E. van Wijk,  
857 K., Wilson, T.M., Cronin, S.J., Leonard, G.S., Lindsay, J.M., Németh, K., Smith, I.E.M.,  
858 2020. Auckland Volcanic Field magmatism, volcanism, and hazard: a review, *New Zealand  
859 Journal of Geology and Geophysics*, DOI: 10.1080/00288306.2020.1736102
- 860 Howell, D.G., 1980. Mesozoic accretion of exotic terranes along the New Zealand segment of  
861 Gondwanaland. *Geology* 8, 487-491.
- 862 Hunt, T., 1978. Stokes magnetic anomaly system. *New Zealand journal of geology and  
863 geophysics* 21, 595-606.
- 864 Jackson, C.A.L., 2012. Seismic reflection imaging and controls on the preservation of ancient  
865 sill-fed magmatic vents. *Journal of the Geological Society* 169, 503.

- 866 Johnston, M.R., 2019. Chapter 2 The path to understanding the central terranes of  
867 Zealandia. Geological Society, London, Memoirs 49, 15-30.
- 868 Kaislaniemi, L., van Hunen, J., Allen, M.B., Neill, I., 2014. Sublithospheric small-scale  
869 convection—A mechanism for collision zone magmatism. *Geology* 42, 291-294.
- 870 Kallweit, R.S., Wood, L.C., 1982. The limits of resolution of zero-phase wavelets.  
871 *Geophysics* 47, 1035-1046.
- 872 Kavanagh, J.L., Menand, T., Sparks, R.S.J., 2006. An experimental investigation of sill  
873 formation and propagation in layered elastic media. *Earth and Planetary Science Letters* 245,  
874 799-813.
- 875 Kenny, J.A., Lindsay, J.M., Howe, T.M., 2012. Post-Miocene faults in Auckland: insights  
876 from borehole and topographic analysis. *New Zealand Journal of Geology and Geophysics*  
877 55, 323-343.
- 878 Killops, S.D., Cook, R.A., Sykes, R., Boudou, J.P., 1997. Petroleum potential and oil-source  
879 correlation in the Great South and Canterbury Basins. *New Zealand Journal of Geology and*  
880 *Geophysics* 40, 405-423.
- 881 Kula, J., Tulloch, A., Spell, T.L., Wells, M.L., 2007. Two-stage rifting of Zealandia-  
882 Australia-Antarctica: Evidence from  $^{40}\text{Ar}/^{39}\text{Ar}$  thermochronometry of the Sisters shear  
883 zone, Stewart Island, New Zealand. *Geology* 35, 411-414.
- 884 Laird, M.G., Bradshaw, J.D., 2004. The Break-up of a Long-term Relationship: the  
885 Cretaceous Separation of New Zealand from Gondwana. *Gondwana Research* 7, 273-286.
- 886 Lamb, S., Mortimer, N., Smith, E., Turner, G., 2016. Focusing of relative plate motion at a  
887 continental transform fault: Cenozoic dextral displacement >700 km on New Zealand's  
888 Alpine Fault, reversing >225 km of Late Cretaceous sinistral motion. *Geochemistry,*  
889 *Geophysics, Geosystems* 17, 1197-1213.
- 890 Le Corvec, N., Bebbington, M. S., Lindsay, J. M., and McGee, L. E. ( 2013), Age, distance,  
891 and geochemical evolution within a monogenetic volcanic field: Analyzing patterns in the  
892 Auckland Volcanic Field eruption sequence, *Geochem. Geophys. Geosyst.*, 14, 3648– 3665,  
893 doi:10.1002/ggge.20223.
- 894 Ledevin, M., Arndt, N., Cooper, M.R., Earls, G., Lyle, P., Aubourg, C., Lewin, E., 2012.  
895 Intrusion history of the Portrush Sill, County Antrim, Northern Ireland: evidence for rapid  
896 emplacement and high-temperature contact metamorphism. *Geological Magazine* 149, 67-79.
- 897 Lindsay, J.M., Leonard, G.S., Smid, E.R., Hayward, B.W., 2011. Age of the Auckland  
898 Volcanic Field: a review of existing data. *New Zealand Journal of Geology and Geophysics*  
899 54, 379-401.

- 900 Lu, H., Fulthorpe, C.S., 2004. Controls on sequence stratigraphy of a middle Miocene–  
901 Holocene, current-swept, passive margin: Offshore Canterbury Basin, New Zealand. GSA  
902 Bulletin 116, 1345-1366.
- 903 Magee, C., Briggs, F., Jackson, C.A.L., 2013a. Lithological controls on igneous intrusion-  
904 induced ground deformation. *Journal of the Geological Society* 170, 853.
- 905 Magee, C., Ernst, R.E., Muirhead, J., Phillips, T., Jackson, C.A.-L., 2019. Magma Transport  
906 Pathways in Large Igneous Provinces: Lessons from Combining Field Observations and  
907 Seismic Reflection Data, *Dyke Swarms of the World: A Modern Perspective*. Springer, pp.  
908 45-85.
- 909 Magee, C., Hunt-Stewart, E., Jackson, C.A.L., 2013b. Volcano growth mechanisms and the  
910 role of sub-volcanic intrusions: Insights from 2D seismic reflection data. *Earth and Planetary  
911 Science Letters* 373, 41-53.
- 912 Magee, C., Jackson, C.A.-L., How do normal faults grow above dykes? EarthArXiv.
- 913 Magee, C., Jackson, C.A.L., 2020. Seismic reflection data reveal the 3D structure of the  
914 newly discovered Exmouth Dyke Swarm, offshore NW Australia. EarthArXiv.
- 915 Magee, C., Jackson, C.A.L., Hardman, J.P., Reeve, M.T., 2017. Decoding sill emplacement  
916 and forced fold growth in the Exmouth Sub-basin, offshore northwest Australia: Implications  
917 for hydrocarbon exploration. *Interpretation* 5, SK11-SK22.
- 918 Magee, C., Maharaj, S.M., Wrona, T. and Jackson, C.A.L., 2015. Controls on the expression  
919 of igneous intrusions in seismic reflection data. *Geosphere*, 11(4), pp.1024-1041.  
920 doi:10.1130/GES01150.1
- 921 Magee, C., Muirhead, J.D., Karvelas, A., Holford, S.P., Jackson, C.A.L., Bastow, I.D.,  
922 Schofield, N., Stevenson, C.T.E., McLean, C., McCarthy, W., Shtukert, O., 2016. Lateral  
923 magma flow in mafic sill complexes. *Geosphere* 12, 809-841.
- 924 Magee, C., Stevenson, C.T.E., Ebmeier, S.K., Keir, D., Hammond, J.O.S., Gottsmann, J.H.,  
925 Whaler, K.A., Schofield, N., Jackson, C.A.L., Petronis, M.S., O'Driscoll, B., Morgan, J.,  
926 Cruden, A., Vollgger, S.A., Dering, G., Micklethwaite, S., Jackson, M.D., 2018. Magma  
927 Plumbing Systems: A Geophysical Perspective. *Journal of Petrology* 59, 1217-1251.
- 928 Maresh, J., White, R.S., Hobbs, R.W., Smallwood, J.R., 2006. Seismic attenuation of Atlantic  
929 margin basalts: Observations and modeling. *Geophysics* 71, B211-B221.
- 930 Mazarini, F., 2007. Vent distribution and crustal thickness in stretched continental crust: The  
931 case of the Afar Depression (Ethiopia). *Geosphere* 3, 152-162.



- 932 McGee, L.E., Smith, I.E.M., Millet, M.-A., Handley, H.K., Lindsay, J.M., 2013.  
933 Asthenospheric Control of Melting Processes in a Monogenetic Basaltic System: a Case  
934 Study of the Auckland Volcanic Field, New Zealand. *Journal of Petrology* 54, 2125-2153.
- 935 McLean, C.E., Schofield, N., Brown, D.J., Jolley, D.W., Reid, A., 2017. 3D seismic imaging  
936 of the shallow plumbing system beneath the Ben Nevis Monogenetic Volcanic Field: Faroe–  
937 Shetland Basin. *Journal of the Geological Society* 174, 468.
- 938 Menand, T., 2011. Physical controls and depth of emplacement of igneous bodies: A  
939 review. *Tectonophysics*, 500(1-4), pp.11-19.
- 940 Morewood, N.C., Shannon, P.M., Mackenzie, G.D., 2004. Seismic stratigraphy of the  
941 southern Rockall Basin: a comparison between wide-angle seismic and normal incidence  
942 reflection data. *Marine and Petroleum Geology* 21, 1149-1163.
- 943 Morgan, W.J., 1972. Deep mantle convection plumes and plate motions. *AAPG bulletin* 56,  
944 203-213.
- 945 Morley, C.K., 2018. 3-D seismic imaging of the plumbing system of the Kora Volcano,  
946 Taranaki Basin, New Zealand: The influence of syn-rift structure on shallow igneous  
947 intrusion architecture. *Geosphere* 14, 2533-2584.
- 948 Morley, C.K., Maczak, A., Rungprom, T., Ghosh, J., Cartwright, J.A., Bertoni, C.,  
949 Panpichityota, N., 2017. New style of honeycomb structures revealed on 3D seismic data  
950 indicate widespread diagenesis offshore Great South Basin, New Zealand. *Marine and*  
951 *Petroleum Geology* 86, 140-154.
- 952 Mortimer, N., 2004. New Zealand's Geological Foundations. *Gondwana Research* 7, 261-  
953 272.
- 954 Mortimer, N., Davey, F.J., Melhuish, A., Yu, J., Godfrey, N.J., 2002. Geological  
955 interpretation of a deep seismic reflection profile across the Eastern Province and Median  
956 Batholith, New Zealand: Crustal architecture of an extended Phanerozoic convergent orogen.  
957 *New Zealand Journal of Geology and Geophysics* 45, 349-363.
- 958 Mortimer, N., Rattenbury, M.S., King, P.R., Bland, K.J., Barrell, D.J.A., Bache, F., Begg,  
959 J.G., Campbell, H.J., Cox, S.C., Crampton, J.S., Edbrooke, S.W., Forsyth, P.J., Johnston,  
960 M.R., Jongens, R., Lee, J.M., Leonard, G.S., Raine, J.I., Skinner, D.N.B., Timm, C.,  
961 Townsend, D.B., Tulloch, A.J., Turnbull, I.M., Turnbull, R.E., 2014. High-level stratigraphic  
962 scheme for New Zealand rocks. *New Zealand Journal of Geology and Geophysics* 57, 402-  
963 419.
- 964 Mortimer, N., Tulloch, A.J., Spark, R.N., Walker, N.W., Ladley, E., Allibone, A.,  
965 Kimbrough, D.L., 1999. Overview of the Median Batholith, New Zealand: a new  
966 interpretation of the geology of the Median Tectonic Zone and adjacent rocks. *Journal of*  
967 *African Earth Sciences* 29, 257-268.

- 968 Mortimer, N., van den Bogaard, P., Hoernle, K., Timm, C., Gans, P.B., Werner, R., Riefstahl,  
969 F., 2019. Late Cretaceous oceanic plate reorganization and the breakup of Zealandia and  
970 Gondwana. *Gondwana Research* 65, 31-42.
- 971 Muir, R.J., Bradshaw, J.D., Weaver, S.D., Laird, M.G., 2000. The influence of basement  
972 structure on the evolution of the Taranaki Basin, New Zealand. *Journal of the Geological*  
973 *Society* 157, 1179.
- 974 Németh, K., 2010. Monogenetic volcanic fields: Origin, sedimentary record, and relationship  
975 with polygenetic volcanism, in: Cañón-Tapia, E., Szakács, A. (Eds.), *What Is a Volcano?*  
976 *Geological Society of America*, p. 0.
- 977 Németh, K., White, J.D.L., 2003. Reconstructing eruption processes of a Miocene  
978 monogenetic volcanic field from vent remnants: Waipiata Volcanic Field, South Island, New  
979 Zealand. *Journal of Volcanology and Geothermal Research* 124, 1-21.
- 980 Németh, K., White, J.D.L., Reay, A., Martin, U., 2003. Compositional variation during  
981 monogenetic volcano growth and its implications for magma supply to continental volcanic  
982 fields. *Journal of the Geological Society* 160, 523.
- 983 Patruno, S., Helland-Hansen, W., 2018. Clinofolds and clinofold systems: Review and  
984 dynamic classification scheme for shorelines, subaqueous deltas, shelf edges and continental  
985 margins. *Earth-Science Reviews* 185, 202-233.
- 986 Phillips, T.B., McCaffrey, K.J., 2019. Terrane boundary reactivation, barriers to lateral fault  
987 propagation and reactivated fabrics - Rifting across the Median Batholith Zone, Great South  
988 Basin, New Zealand. *Tectonics* 0.
- 989 Planke, S., Rasmussen, T., Rey, S.S., Myklebust, R., 2005. Seismic characteristics and  
990 distribution of volcanic intrusions and hydrothermal vent complexes in the Vøring and Møre  
991 basins. *Geological Society, London, Petroleum Geology Conference*  
992 series 6, 833.
- 993 Planke, S., Symonds, P.A., Alvestad, E., Skogseid, J., 2000. Seismic volcanostratigraphy of  
994 large-volume basaltic extrusive complexes on rifted margins. *Journal of Geophysical*  
995 *Research: Solid Earth* 105, 19335-19351.
- 996 Polteau, S., Ferré, E.C., Planke, S., Neumann, E.R., Chevallier, L., 2008. How are saucer-  
997 shaped sills emplaced? Constraints from the Golden Valley Sill, South Africa. *Journal of*  
998 *Geophysical Research: Solid Earth* 113.
- 999 Price, R., Chappell, B., 1975. Fractional crystallisation and the petrology of Dunedin  
1000 Volcano. *Contributions to mineralogy and petrology* 53, 157-182.
- 1001 Pryer, L., Weir, J., Debacker, T., Romine, K., 2013. Interpretation of basement: NZ ECS  
1002 SEEBASE: Advantage New Zealand Petroleum Summit. April.

- 1003 Quirie, A.K., Schofield, N., Hartley, A., Hole, M.J., Archer, S.G., Underhill, J.R., Watson,  
1004 D., Holford, S.P., 2019. The Rattray Volcanics: Mid-Jurassic fissure volcanism in the UK  
1005 Central North Sea. *Journal of the Geological Society* 176, 462-481.
- 1006 Rawlinson, N., Davies, D.R., Pilia, S., 2017. The mechanisms underpinning Cenozoic  
1007 intraplate volcanism in eastern Australia: Insights from seismic tomography and geodynamic  
1008 modeling. *Geophysical Research Letters* 44, 9681-9690.
- 1009 Reeves, J., Magee, C., Jackson, C., 2018. Unravelling intrusion-induced forced fold  
1010 kinematics and ground deformation using 3D seismic reflection data. *Volcanica*, 1-17.
- 1011 Reynolds, P., Holford, S., Schofield, N., Ross, A., 2017. Three-Dimensional Seismic Imaging  
1012 of Ancient Submarine Lava Flows: An Example From the Southern Australian Margin.  
1013 *Geochemistry, Geophysics, Geosystems* 18, 3840-3853.
- 1014 Reynolds, P., Schofield, N., Brown, R.J., Holford, S.P., 2018. The architecture of submarine  
1015 monogenetic volcanoes – insights from 3D seismic data. *Basin Res* 30, 437-451.
- 1016 Robertson, A.H.F., Campbell, H.J., Johnston, M.R., Palamakumbra, R., 2019. Chapter 15  
1017 Construction of a Paleozoic–Mesozoic accretionary orogen along the active continental  
1018 margin of SE Gondwana (South Island, New Zealand): summary and overview. *Geological*  
1019 *Society, London, Memoirs* 49, 331-372.
- 1020 Rout, D.J., Cassidy, J., Locke, C.A., Smith, I.E.M., 1993. Geophysical evidence for temporal  
1021 and structural relationships within the monogenetic basalt volcanoes of the Auckland  
1022 volcanic field, northern New Zealand. *Journal of Volcanology and Geothermal Research* 57,  
1023 71-83.
- 1024 Sahoo, T., King, P., Bland, K., Strogen, D., Sykes, R., Bache, F., 2014. Tectono-sedimentary  
1025 evolution and source rock distribution of the mid to Late Cretaceous succession in the Great  
1026 South Basin, New Zealand *The APPEA Journal* 54, 259-274.
- 1027 Schofield, N., Holford, S., Millett, J., Brown, D., Jolley, D., Passey, S.R., Muirhead, D.,  
1028 Grove, C., Magee, C., Murray, J. and Hole, M., 2017. Regional magma plumbing and  
1029 emplacement mechanisms of the Faroe-Shetland Sill Complex: implications for magma  
1030 transport and petroleum systems within sedimentary basins. *Basin Research*, 29(1), pp.41-63.
- 1031 Slatt, R.M., 2006. Stratigraphic reservoir characterization for petroleum geologists,  
1032 geophysicists, and engineers. Elsevier.
- 1033 Sleep, N.H., 1992. Hotspot volcanism and mantle plumes. *Annual Review of Earth and*  
1034 *Planetary Sciences* 20, 19-43.
- 1035 Smallwood, J.R., Maresh, J., 2002. The properties, morphology and distribution of igneous  
1036 sills: modelling, borehole data and 3D seismic from the Faroe-Shetland area. *Geological*  
1037 *Society, London, Special Publications* 197, 271.

- 1038 Speight, R., 1943. The geology of Banks Peninsula: a revision, Transactions of the New  
1039 Zealand Institute, pp. 13-26.
- 1040 Spörli, K.B., Black, P.M., Lindsay, J.M., 2015. Excavation of buried Dun Mountain–Maitai  
1041 terrane ophiolite by volcanoes of the Auckland Volcanic field, New Zealand. New Zealand  
1042 Journal of Geology and Geophysics 58, 229-243.
- 1043 Spörli, K.B., Eastwood, V.R., 1997. Elliptical boundary of an intraplate volcanic field,  
1044 Auckland, New Zealand. Journal of Volcanology and Geothermal Research 79, 169-179.
- 1045 Stephens, T.L., Walker, R.J., Healy, D., Bubeck, A., England, R.W., McCaffrey, K.J.W.,  
1046 2017. Igneous sills record far-field and near-field stress interactions during volcano  
1047 construction: Isle of Mull, Scotland. Earth and Planetary Science Letters 478, 159-174.
- 1048 Stipp, J.J., McDougall, I., 1968. Geochronology of the Banks Peninsula Volcanoes, New  
1049 Zealand. New Zealand Journal of Geology and Geophysics 11, 1239-1258.
- 1050 Sun, Q., Jackson, C.A.L., Magee, C., Mitchell, S.J., Xie, X., 2019a. Extrusion dynamics of  
1051 deep-water volcanoes. Solid Earth Discuss. 2019, 1-40.
- 1052 Sun, Q., Jackson, C.A., Magee, C. and Xie, X., 2020. Deeply buried ancient volcanoes  
1053 control hydrocarbon migration in the South China Sea. *Basin Research*, 32(1), pp.146-162
- 1054 Sutherland, R., 1995. The Australia-Pacific boundary and Cenozoic plate motions in the SW  
1055 Pacific: Some constraints from Geosat data. Tectonics 14, 819-831.
- 1056 Sutherland, R., 1999. Basement geology and tectonic development of the greater New  
1057 Zealand region: an interpretation from regional magnetic data. Tectonophysics 308, 341-362.
- 1058 Symonds, P.A., Planke, S., Frey, O., Skogseid, J., 1998. Volcanic evolution of the Western  
1059 Australian continental margin and its implications for basin development.
- 1060 Tarling, M.S., Smith, S.A.F., Scott, J.M., Rooney, J.S., Viti, C., Gordon, K.C., 2019. The  
1061 internal structure and composition of a plate-boundary-scale serpentinite shear zone: the  
1062 Livingstone Fault, New Zealand. Solid Earth 10, 1025-1047.
- 1063 Thomson, K., 2005. Volcanic features of the North Rockall Trough: application of  
1064 visualisation techniques on 3D seismic reflection data. Bulletin of Volcanology 67, 116-128.
- 1065 Thomson, K., Hutton, D., 2004. Geometry and growth of sill complexes: insights using 3D  
1066 seismic from the North Rockall Trough. Bulletin of Volcanology 66, 364-375.
- 1067 Timm, C., Hoernle, K., Van Den Bogaard, P., Bindeman, I., Weaver, S., 2009. Geochemical  
1068 Evolution of Intraplate Volcanism at Banks Peninsula, New Zealand: Interaction Between  
1069 Asthenospheric and Lithospheric Melts. Journal of Petrology 50, 989-1023.

- 1070 Timm, C., Hoernle, K., Werner, R., Hauff, F., den Bogaard, P.v., White, J., Mortimer, N.,  
1071 Garbe-Schönberg, D., 2010. Temporal and geochemical evolution of the Cenozoic intraplate  
1072 volcanism of Zealandia. *Earth-Science Reviews* 98, 38-64.
- 1073 Trude, J., Cartwright, J., Davies, R.J., Smallwood, J., 2003. New technique for dating igneous  
1074 sills. *Geology* 31, 813-816.
- 1075 Tulloch, A., Mortimer, N., Ireland, T., Waight, T., Maas, R., Palin, M., Sahoo, T., Seebeck,  
1076 H., Sagar, M., Barrier, A., Turnbull, R., 2019. Reconnaissance basement geology and  
1077 tectonics of South Zealandia. *Tectonics* 0.
- 1078 Uruski, C., 2015. The contribution of offshore seismic data to understanding the evolution of  
1079 the New Zealand continent. *Geol Soc Spec Publ* 413, 35-51.
- 1080 Uruski, C., Kennedy, C., Harrison, T., Maslen, G., Cook, R., Sutherland, R., Zhu, H., 2007.  
1081 Petroleum potential of the Great South Basin, New Zealand—New seismic data improves  
1082 imaging. *The APPEA Journal* 47, 145-161.
- 1083 Uruski, C.I., 2010. New Zealand's deepwater frontier. *Marine and Petroleum Geology* 27,  
1084 2005-2026.
- 1085 Valentine, G.A., Hirano, N., 2010. Mechanisms of low-flux intraplate volcanic fields—Basin  
1086 and Range (North America) and northwest Pacific Ocean. *Geology* 38, 55-58.
- 1087 Waight, T.E., Weaver, S.D., Maas, R., Eby, G.N., 1998. French Creek Granite and Hohonu  
1088 Dyke Swarm, South Island, New Zealand: Late Cretaceous alkaline magmatism and the  
1089 opening of the Tasman Sea. *Australian Journal of Earth Sciences* 45, 823-835.
- 1090 Walker, F., Schofield, N., Millett, J., Jolley, D., Hole, M., Stewart, M., 2019. Paleogene  
1091 volcanic rocks in the northern Faroe-Shetland Basin and Møre Marginal High: Understanding  
1092 lava field stratigraphy. *Geological Society, London, Special Publications* 495, SP495-2019-  
1093 2013.
- 1094 Wall, M., Cartwright, J., Davies, R., McGrandle, A., 2010. 3D seismic imaging of a Tertiary  
1095 Dyke Swarm in the Southern North Sea, UK. *Basin Res* 22, 181-194.
- 1096 Widess, M.B., 1973. How thin is a thin bed? *Geophysics* 38, 1176-1180.
- 1097 Wilson, C., Houghton, B., McWilliams, M., Lanphere, M., Weaver, S., Briggs, R., 1995.  
1098 Volcanic and structural evolution of Taupo Volcanic Zone, New Zealand: a review. *Journal*  
1099 *of volcanology and geothermal research* 68, 1-28.
- 1100 Woodward, D., Hatherton, T., 1975. Magnetic anomalies over southern New Zealand. *New*  
1101 *Zealand journal of geology and geophysics* 18, 65-82.

- 1102 Wright, K.A., Davies, R.J., Jerram, D.A., Morris, J., Fletcher, R., 2012. Application of  
1103 seismic and sequence stratigraphic concepts to a lava-fed delta system in the Faroe-Shetland  
1104 Basin, UK and Faroes. *Basin Res* 24, 91-106.
- 1105 Wright, N.M., Seton, M., Williams, S.E., Müller, R.D., 2016. The Late Cretaceous to recent  
1106 tectonic history of the Pacific Ocean basin. *Earth-Science Reviews* 154, 138-173.
- 1107 Wu, L., Mei, L., Paton, D.A., Guo, P., Liu, Y., Luo, J., Wang, D., Li, M., Zhang, P., Wen, H.,  
1108 2018. Deciphering the origin of the Cenozoic intracontinental rifting and volcanism in eastern  
1109 China using integrated evidence from the Jiangnan Basin. *Gondwana Research* 64, 67-83.
- 1110 Zhao, F., Wu, S., Sun, Q., Huuse, M., Li, W., Wang, Z., 2014. Submarine volcanic mounds in  
1111 the Pearl River Mouth Basin, northern South China Sea. *Marine Geology* 355, 162-172.

1112  
1113

## 1114 **Figure Captions**

1115

1116 Figure 1 – A) Onshore relief and offshore bathymetry map of the South Island of New Zealand  
1117 highlighting the location of the Tuatara Volcanic Field and selected further intraplate volcanic  
1118 products across the South Island. Also shown are the locations of the major terrane boundaries across  
1119 the area (after Mortimer et al 2002). Inset – Map showing the regional basement geology across New  
1120 Zealand. B) Tectono-stratigraphic column showing the major stratigraphy present in the Great South  
1121 Basin, as well as the timings of regional tectonics and volcanism. After Bertoni et al. (2019); Higgs et  
1122 al. (2019); Mortimer et al. (2014).

1123 Figure 2 – A) Magnetic anomaly map across the northern part of the Great South Basin. Data are  
1124 reduced to pole in order to place the anomalies vertically above the magnetic source. The locations of  
1125 major magnetic anomalies are shown after Tulloch et al. (2019) and Sutherland et al. (1999). The  
1126 magnetic data are courtesy of the NZ SEEBASE database (Pryer et al., 2013). B) Two-way-time  
1127 structure map of the top surface of the central edifice of the Tuatara Volcanic Field. The locations of  
1128 prominent volcanic cones are shown by the white triangles. See Figure 1 for location.

1129 Figure 3 – Uninterpreted and interpreted NW-SE oriented seismic section across the Tuatata Volcanic  
1130 Field. The central edifice of the field is identified as a package of high-amplitude reflectivity, with

1131 igneous sills and volcanic cones identified around the main structure. Image quality is greatly reduced  
1132 beneath the main edifice. See Figure 2 for location.

1133 Figure 4 – Uninterpreted and interpreted NE-SW oriented seismic section across the Tuatara Volcanic  
1134 Field. The central edifice (shown in grey) is surrounded by multiple volcanic cones and igneous sills.  
1135 Image quality is greatly reduced beneath the central edifice. See Figure 2 for location.

1136 Figure 5 – Close-up seismic sections and interpretations of the tabular lava sequences that comprise  
1137 the central edifice of the Tuatara Volcanic Field. Stacked lava sequences, individual volcanic cones  
1138 and lava delta sequences are highlighted in the interpretations. See Figure 2 for location.

1139 Figure 6 – Interpreted seismic sections highlighting the morphology and seismic expression of  
1140 volcanic cones within the Tuatara Volcanic Field. See Figure 7 for the locations of individual  
1141 sections.

1142 Figure 7 – A) Map showing the age and distribution of interpreted volcanic cones surrounding the  
1143 Tuatara Volcanic Field. B) Map showing the age of emplacement and distribution of igneous sills  
1144 within and surrounding the Tuatara Volcanic Field. Note that the igneous sills are more widely  
1145 distributed around the central edifice compared to the volcanic cones.

1146 Figure 8 – Uninterpreted and interpreted seismic section showing a minor volcanic cone to the south  
1147 of the main edifice. See Figure 2 for location. Note the presence of Early Eocene aged lava flows  
1148 associated with the volcanic cone.

1149 Figure 9 – Interpreted seismic sections showing a number of different sills interpreted throughout the  
1150 area. See Figure 7 for location. The age of sill emplacement can be estimated as the age of the strata  
1151 onlapping onto the identified forced folds.

1152 Figure 10 – A) Schematic cartoon showing the overall evolution of the Tuatara Volcanic Field. Sill  
1153 emplacement and volcanism begins in the Late Cretaceous, with the majority of activity, including the  
1154 formation of the majority of the central edifice occurring in the Paleocene. Activity migrates towards  
1155 the northwest and wanes throughout the early Eocene, before the Tuatara Field becomes buried. B)

1156 Map showing the distribution of sills and volcanic cones within the Tuatara Volcanic Field. The  
1157 distribution of volcano-magmatic features is co-located with the Livingstone Fault, forming the  
1158 boundary between the Caples and Dun Mountain-Maitai Terranes. Inset – Cartoon showing the setting  
1159 of the Auckland Volcanic Field, located between the same basement terranes on the North Island of  
1160 New Zealand. C) Regional model for the localisation of activity in the Tuatara Volcanic Field. Upper  
1161 crustal basement terranes are based on the SESI seismic section along the east coast of the South  
1162 Island of New, after Mortimer et al. (2002). The lower part of the figure shows the hypothesised  
1163 model for lithosphere detachment and melt generation in the lithosphere. See Figure 1 for location of  
1164 SESI seismic section.

1165 Figure 11 – 3D block model showing the geometry of the Tuatara Volcanic Field and its hypothesised  
1166 link to magma generation at the base of the lithosphere. Areas of detaching material from the base of  
1167 the lithosphere promote decompression melting of upwelling asthenosphere. The detachment of  
1168 lithospheric material progressively migrates northwest-wards along the Livingstone Fault terrane  
1169 boundary, causing the age progression identified in the Tuatara Volcanic Field. The field is thought to  
1170 be dominated by vertical magma transport throughout the lithosphere, and is dominated by sills in the  
1171 upper crust.

1172 Supplementary Figure 1 – Interpreted seismic section linking the study area to the nearby Toroa-1  
1173 borehole, providing age constraints on the shallow sedimentary succession of the Tuatara Volcanic  
1174 Field. Although located a great distance from the study area, the intervening geology between the  
1175 borehole and the Tuatara Volcanic Field is relatively simple, dominated by post-rift strata allowing us  
1176 to correlate horizons across the study area. See Figure 2 for location.

1177



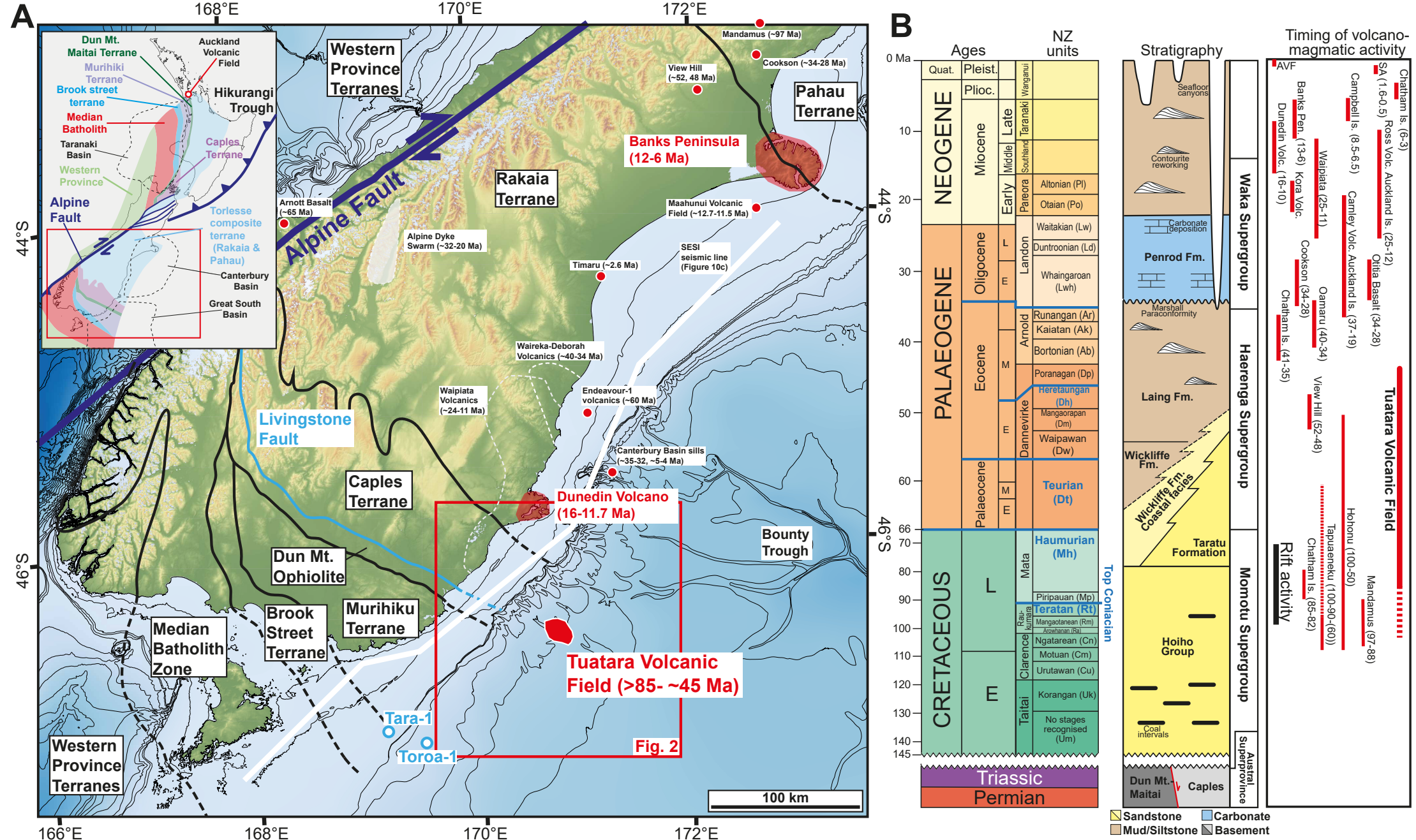
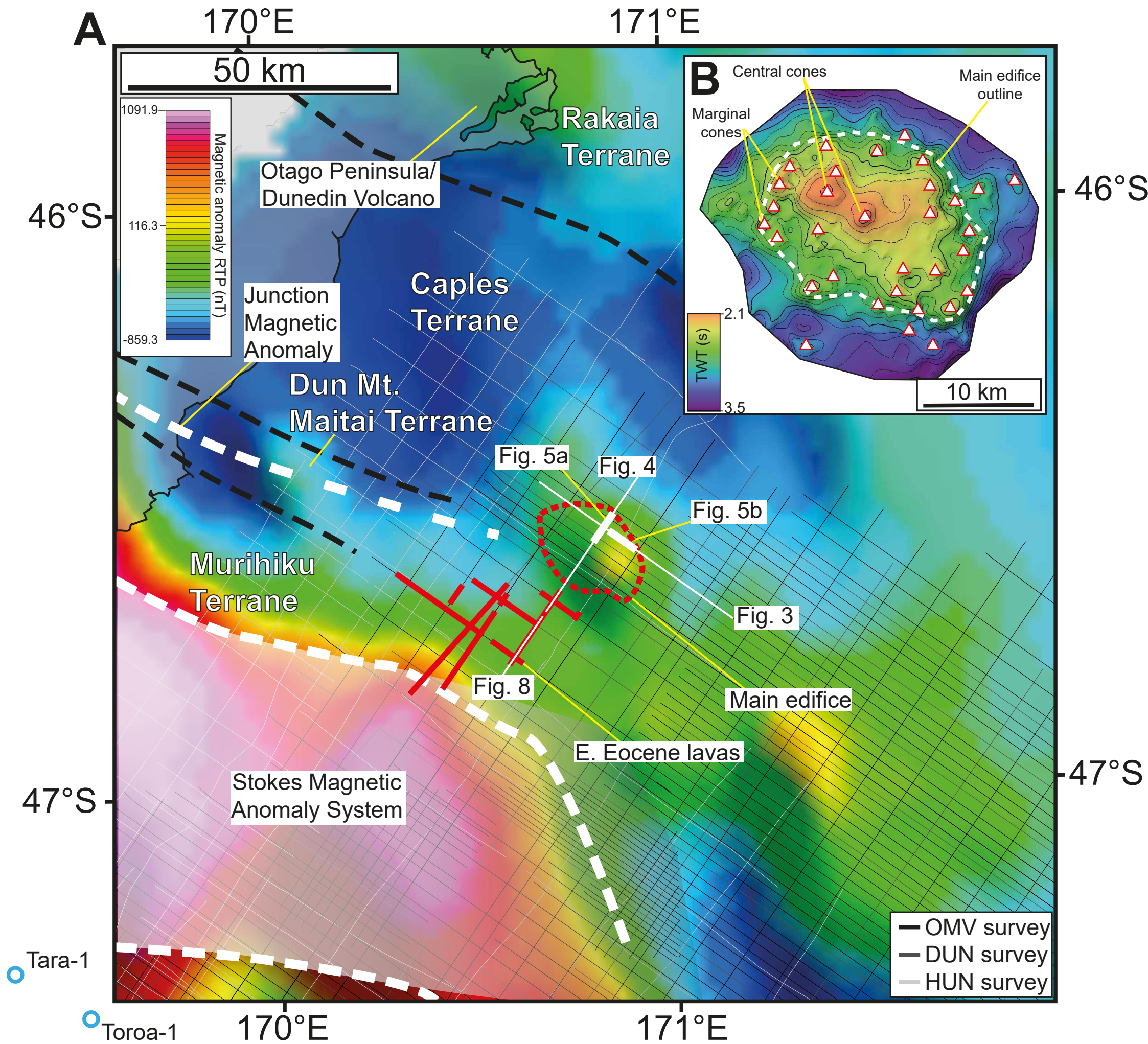


Figure 1





**Figure 2**



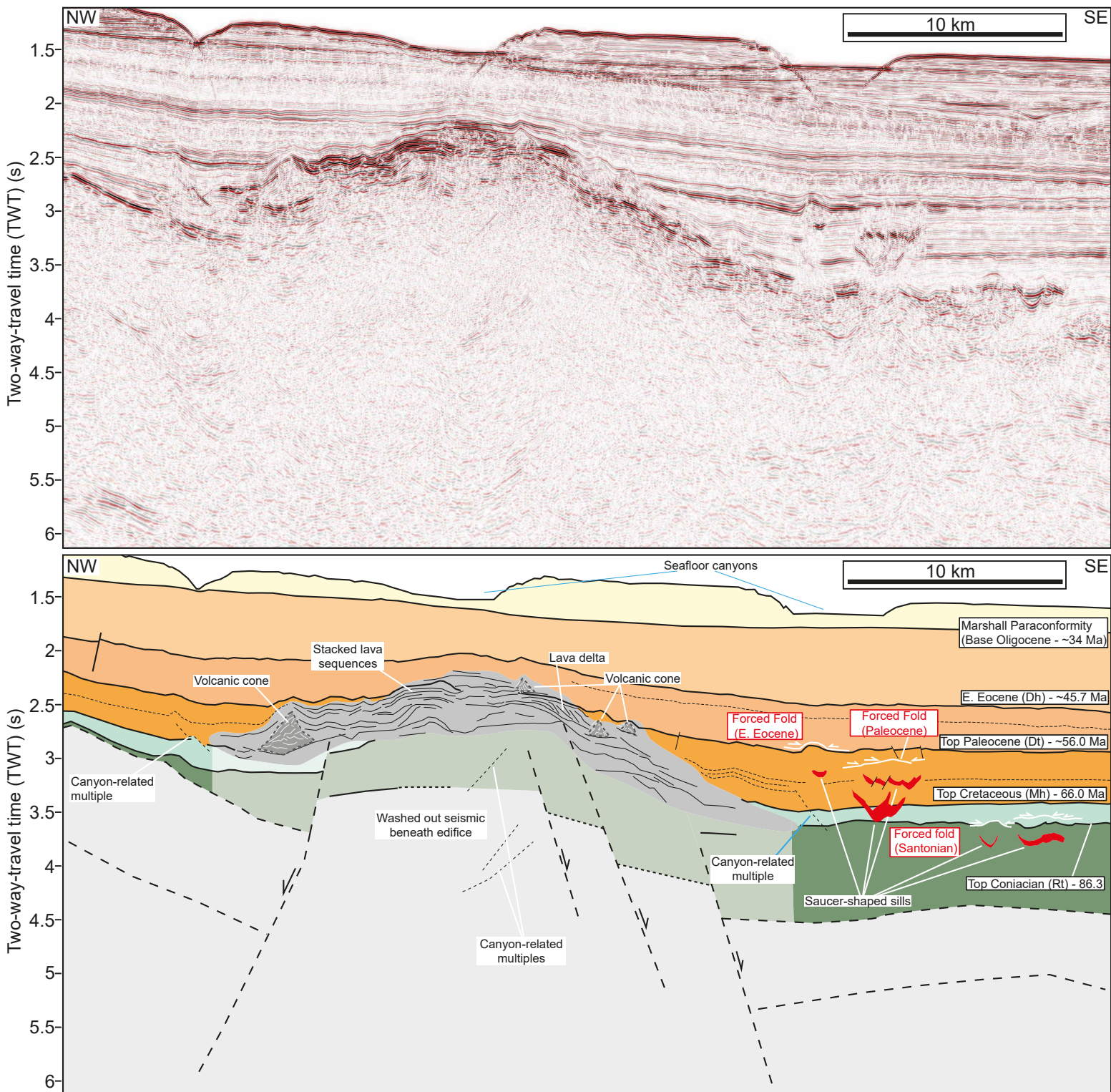


**Figure 3**



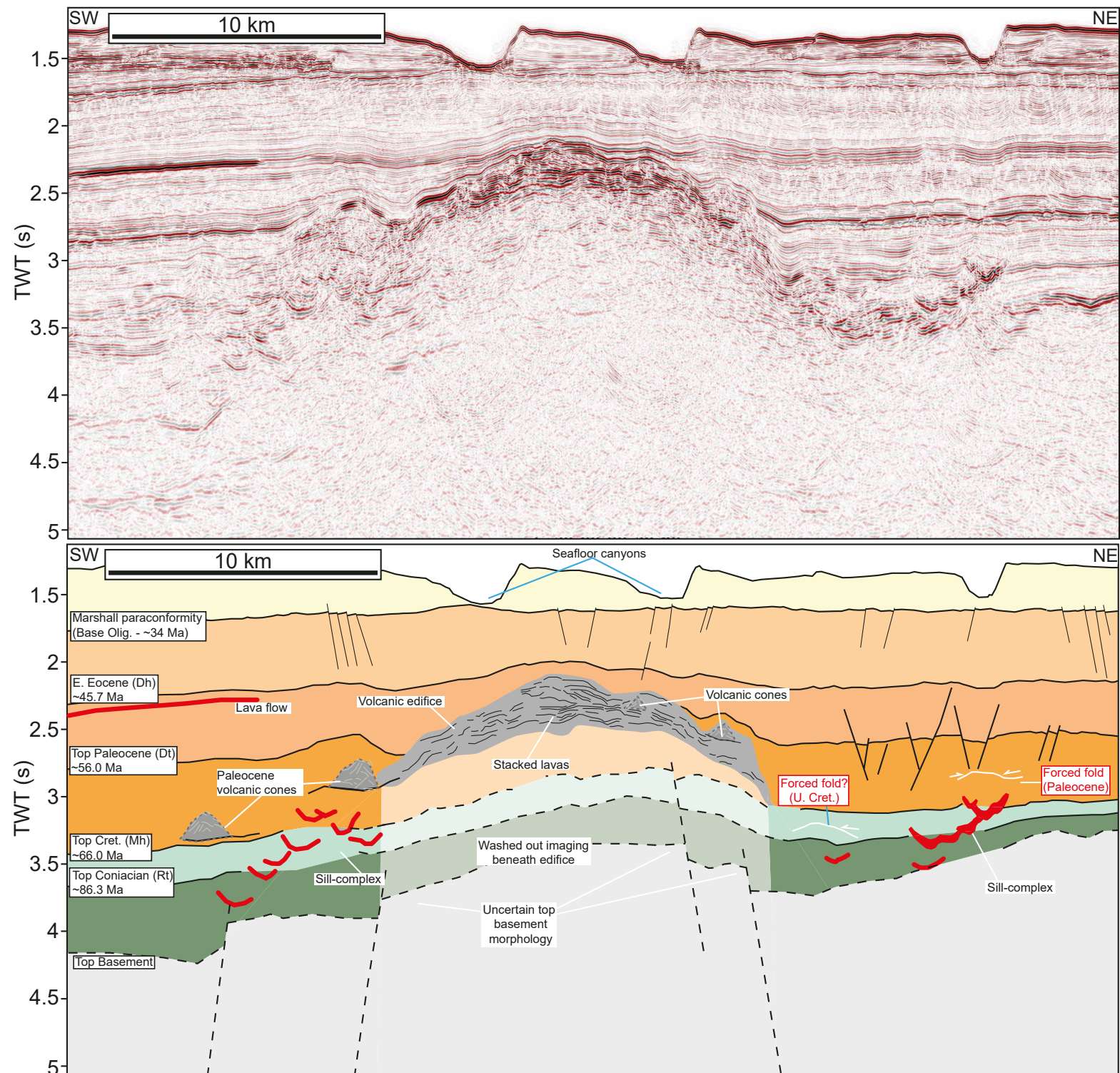
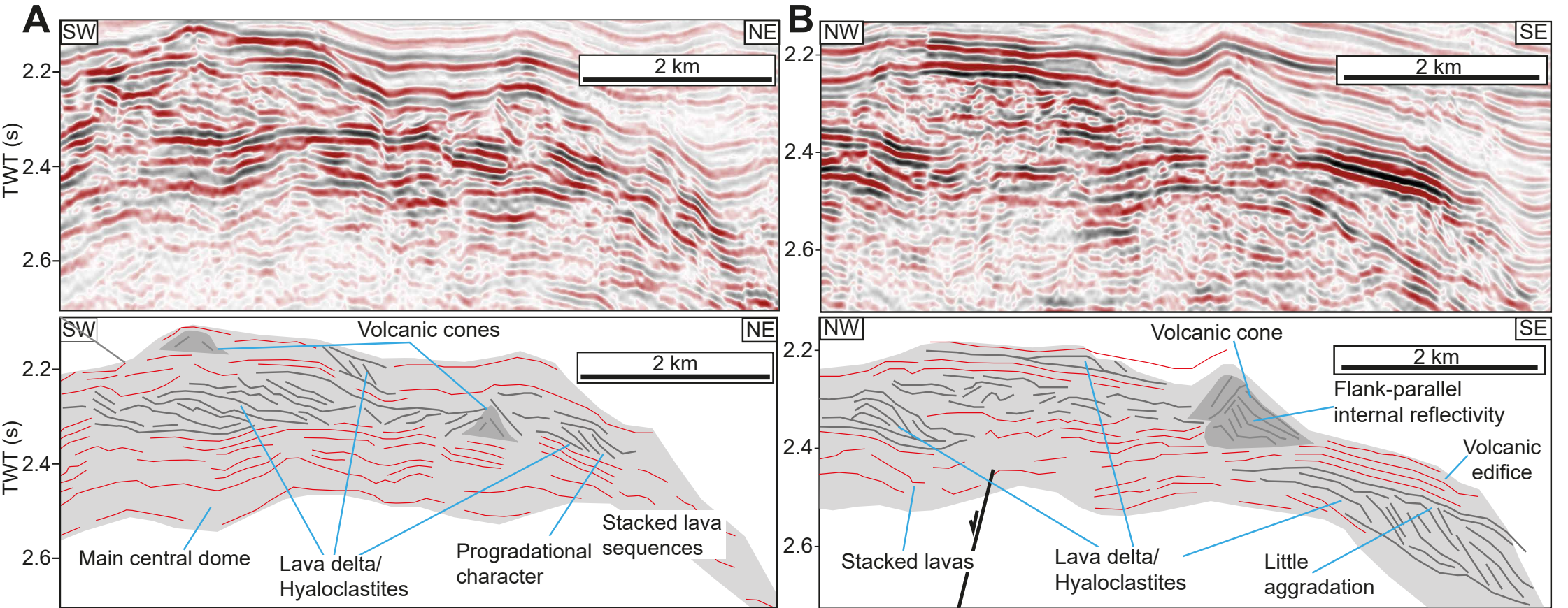


Figure 4



**Figure 5**



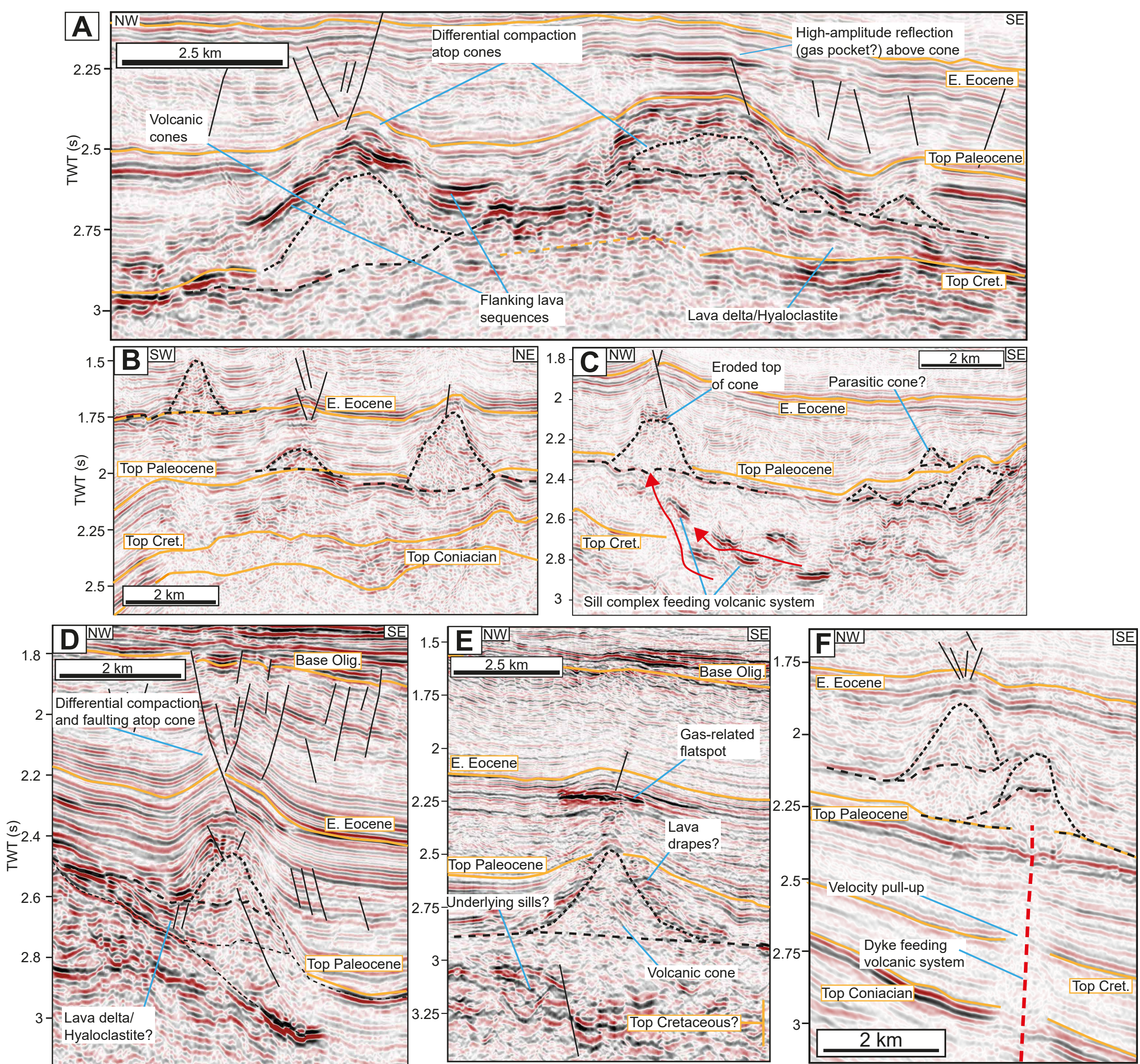


Figure 6



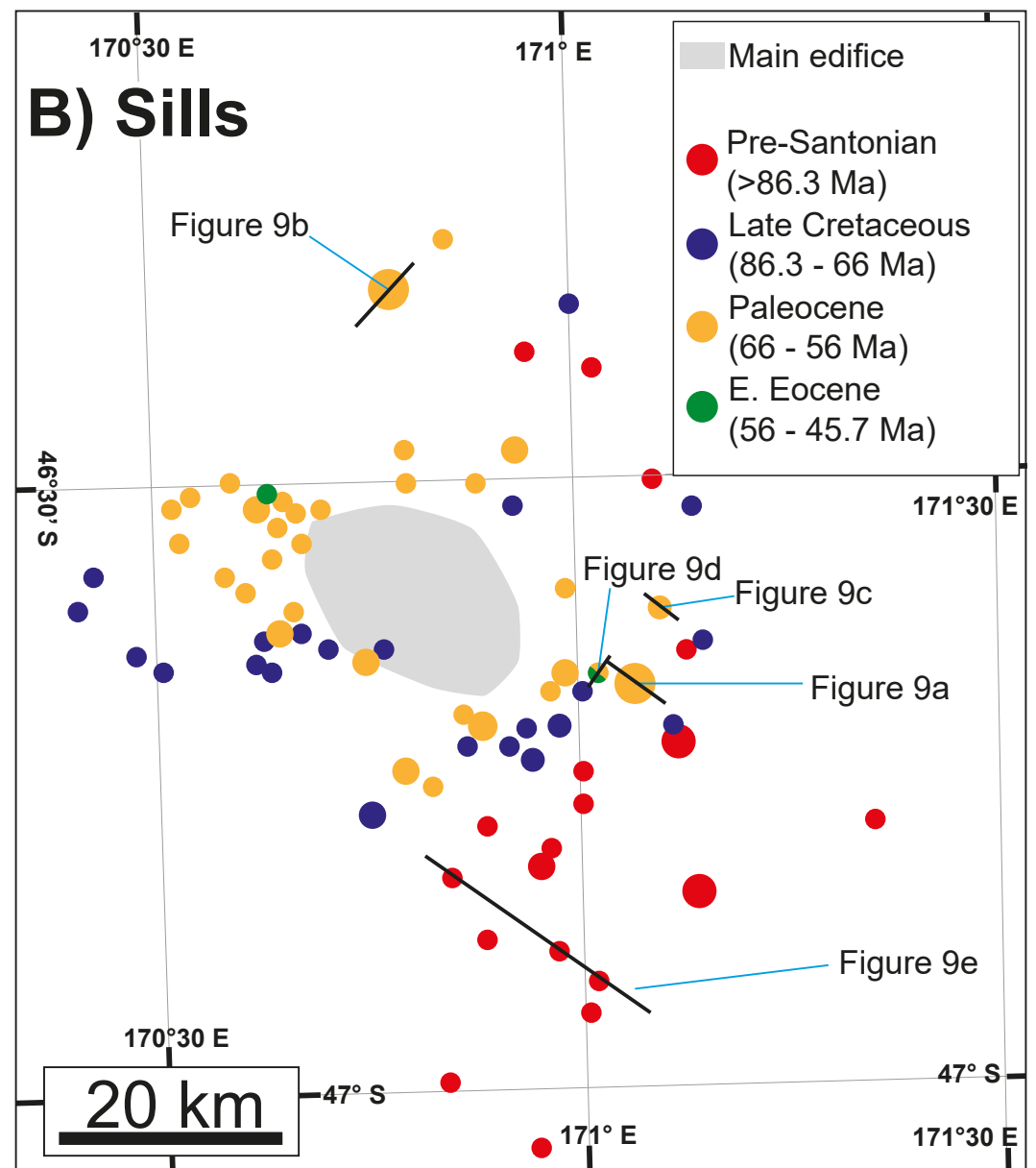
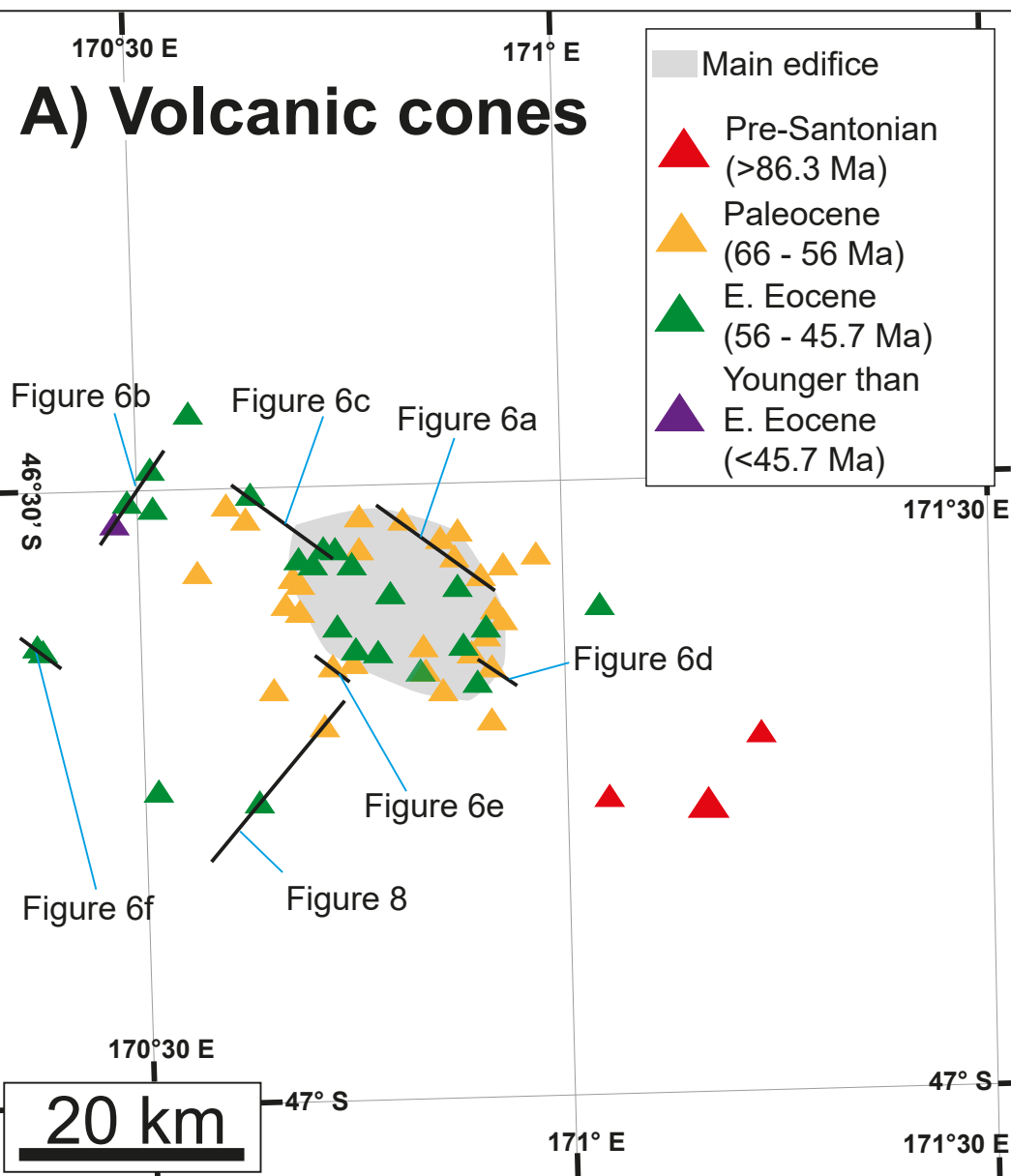


Figure 7



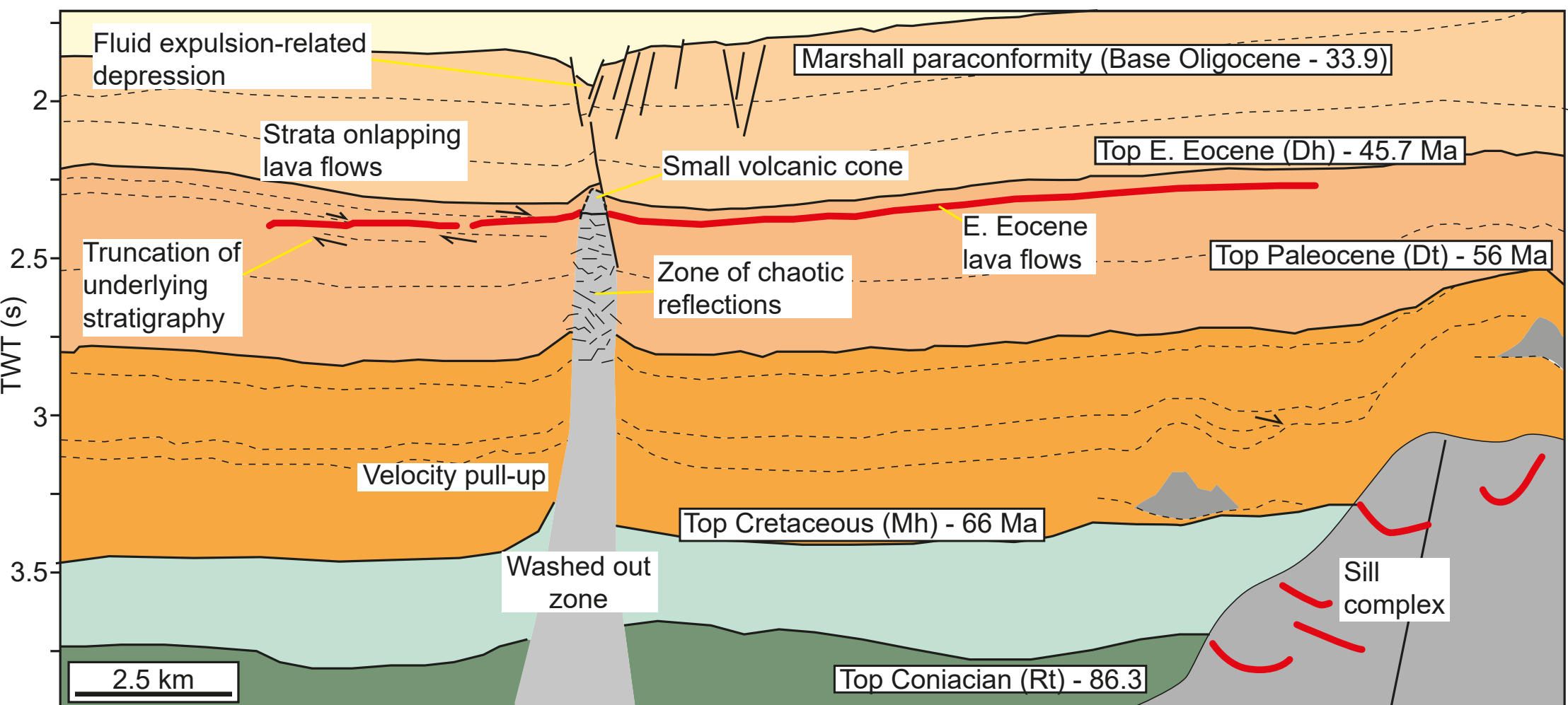
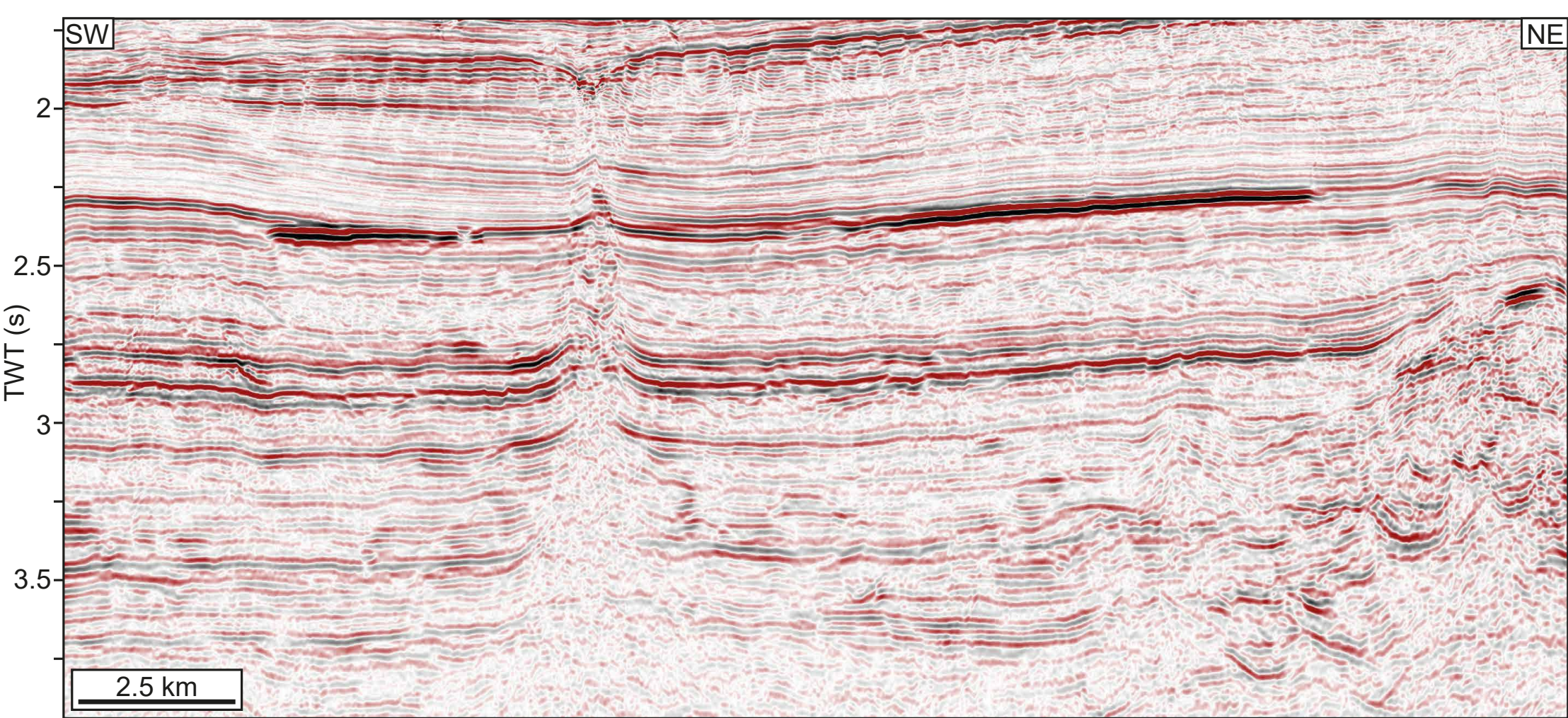


Figure 8



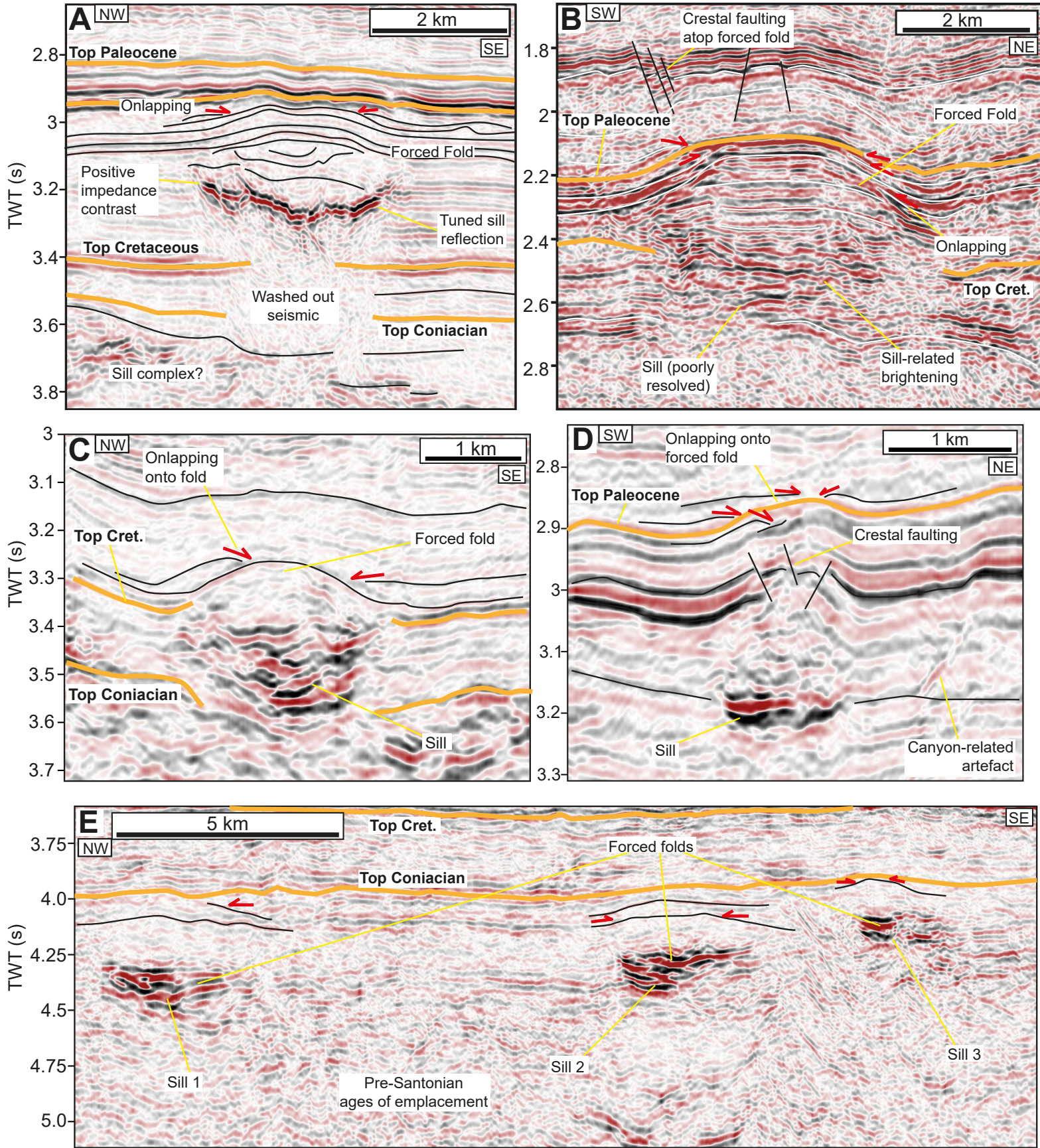


Figure 9



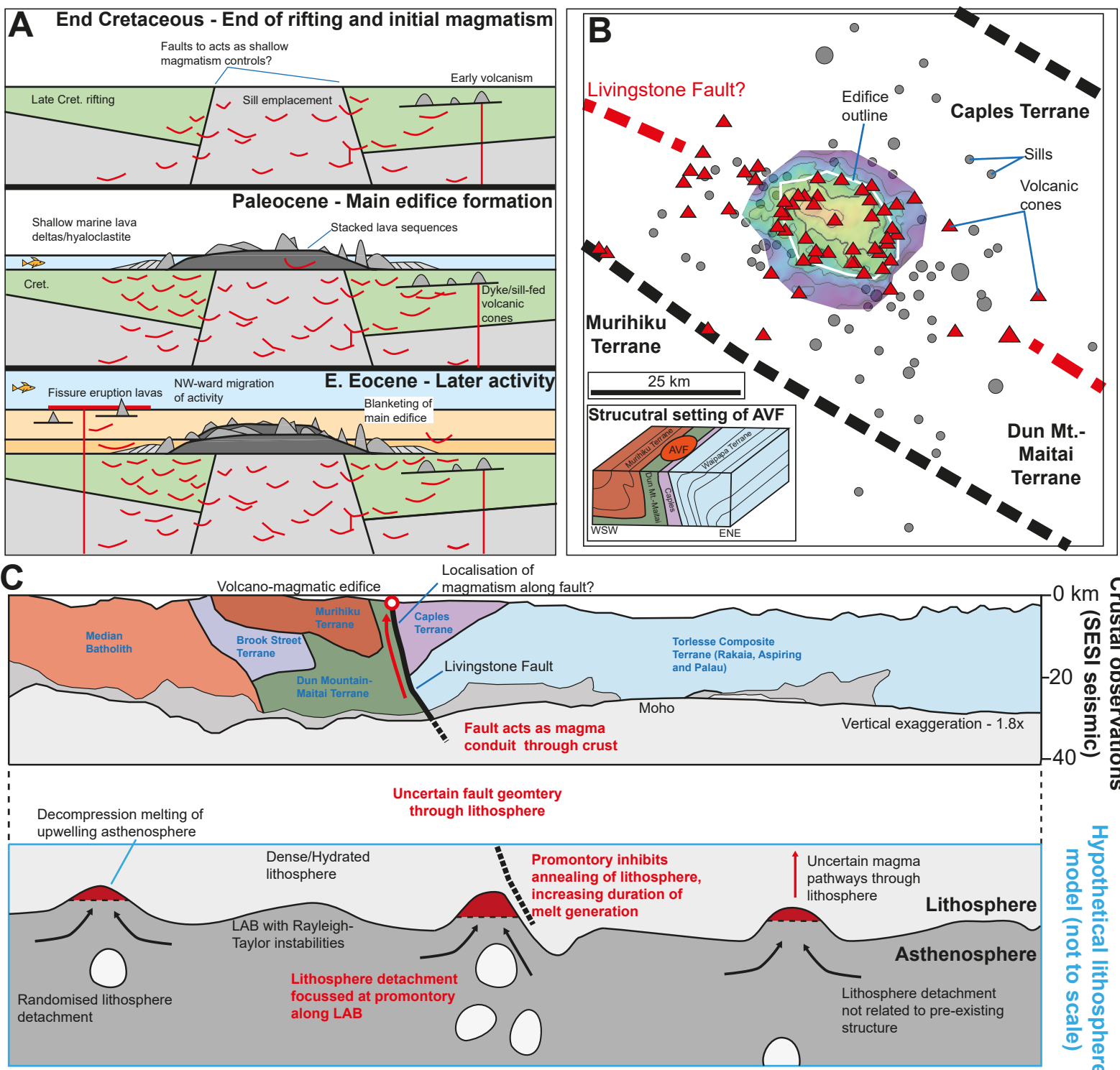
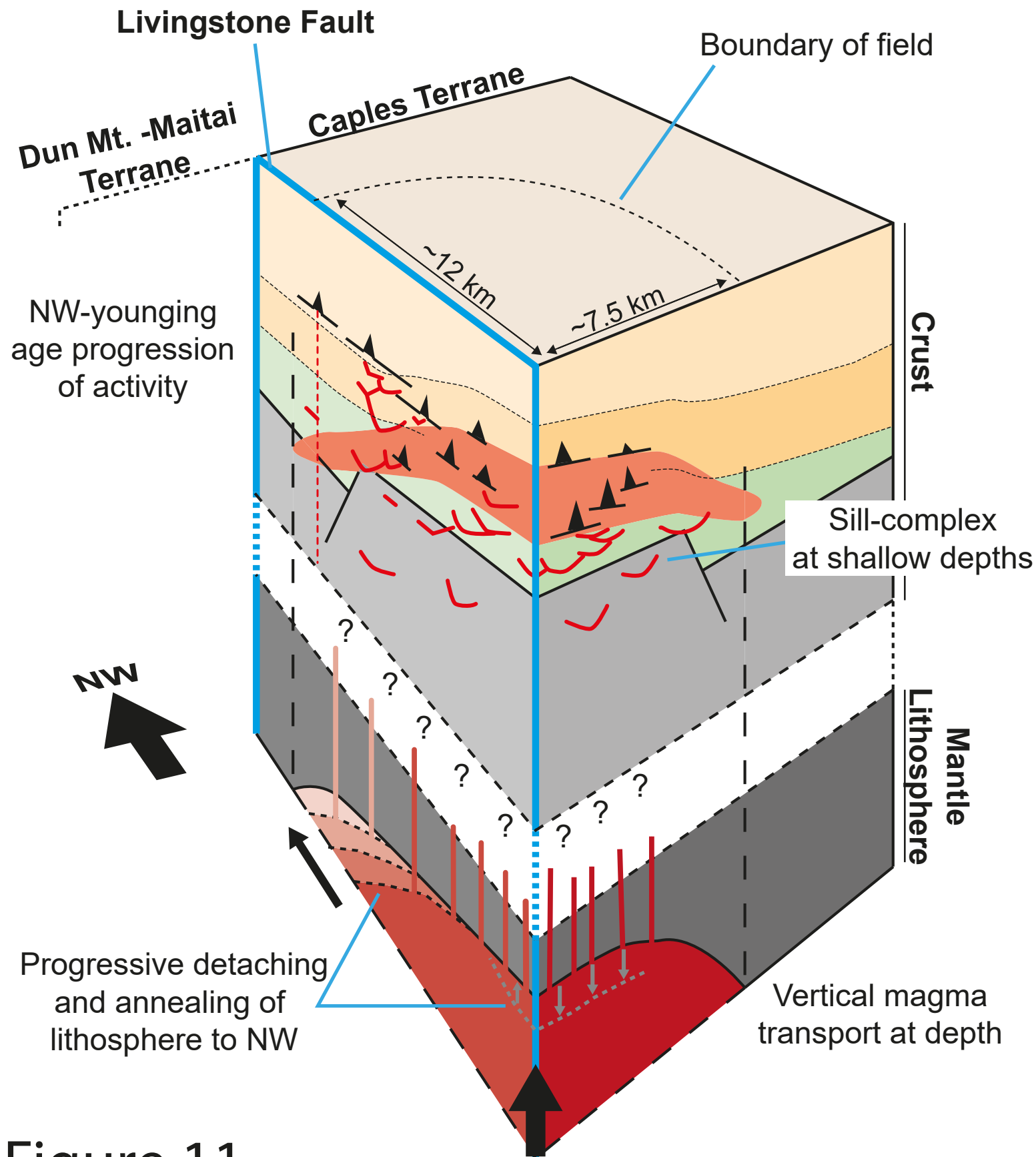
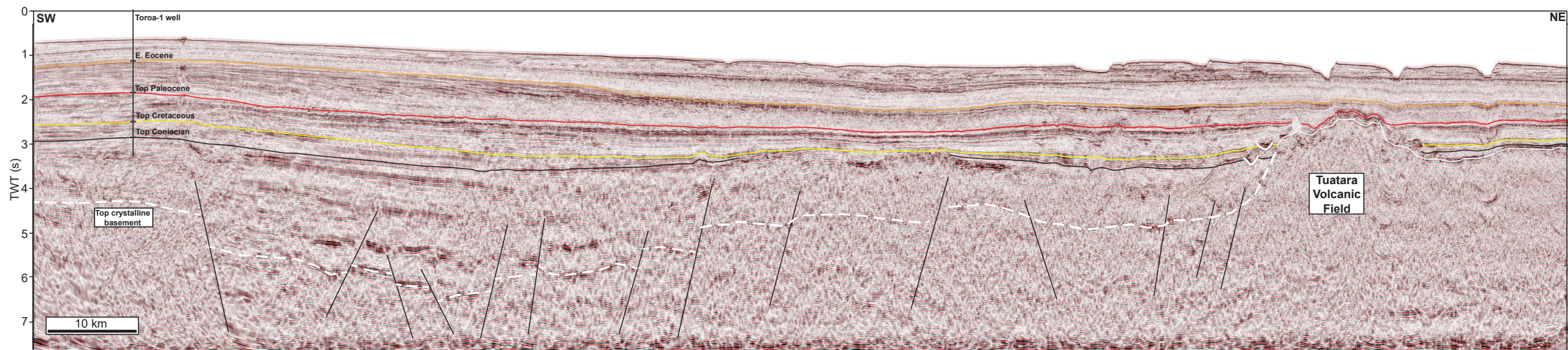


Figure 10



**Figure 11**



Supplementary Figure 1